Available online at www.sciencedirect.com
ScienceDirect
Icarus 195 (2008) 140–168
ICARUS
www.elsevier.com/locate/icarus

Spectral reflectance properties of minerals exposed to simulated Mars surface conditions

E.A. Cloutis [a,*], M.A. Craig [a], R.V. Kruzelecky [b], W.R. Jamroz [b], A. Scott [c], F.C. Hawthorne [d], S.A. Mertzman [e]

[a] *Department of Geography, University of Winnipeg, 515 Portage Avenue, Winnipeg, Manitoba, R3B 2E9, Canada*
[b] *MPB Communications Inc., 147 Hymus Boulevard, Pointe Claire, Quebec, H9R 1E9, Canada*
[c] *COM DEV Ottawa, 303 Terry Fox Drive, Kanata, Ontario, K2K 3J1, Canada*
[d] *Department of Geological Sciences, University of Manitoba, Winnipeg, Manitoba, R3T 2N2, Canada*
[e] *Department of Geosciences, Franklin and Marshall College, Lancaster, PA 17604-3003, USA*

Received 10 September 2007; revised 26 October 2007

Available online 29 January 2008

Abstract

A number of mineral species were exposed to martian surface conditions of atmospheric pressure and composition, temperature, and UV light regime, and their evolution was monitored using reflectance spectroscopy. The stabilities for different groups varied widely. Phyllosilicate spectra all showed measurable losses of interlayer H_2O, with some structural groups showing more rapid H_2O loss than others. Loss of OH from the phyllosilicates is not always accompanied by a change in metal–OH overtone absorption bands. OH-bearing sulfates, such as jarosite and alunite, show no measurable change in spectral properties, suggesting that they should be spectrally detectable on Mars on the basis of diagnostic absorption bands in the 0.4–2.5 μm region. Fe^{3+}- and H_2O-bearing sulfates all showed changes in the appearance and/or reduction in depths of hydroxo-bridged Fe^{3+} absorption bands, particularly at 0.43 μm. The spectral changes were often accompanied by visible color changes, suggesting that subsurface sulfates exposed to the martian surface environment may undergo measurable changes in reflectance spectra and color over short periods of time (days to weeks). Organic-bearing geological materials showed no measurable change in C–H related absorption bands, while carbonates and hydroxides also showed no systematic changes in spectral properties. The addition of ultraviolet irradiation did not seem to affect mineral stability or rate of spectral change, with one exception (hexahydrite). In some cases, spectral changes could be related to the formation of specific new phases. The data also suggest that hydrated minerals detected on Mars to date retain their diagnostic spectral properties that allow their unique identification.

Keywords: Mars, surface; Mineralogy; Spectroscopy

1. Introduction

Spectral reflectance studies of Mars in the reflected portion of the electromagnetic spectrum (here defined as the region below ~3.5 μm) have a long history. The first studies of this sort were done using ground-based telescopes (e.g., Sinton, 1959), and have more recently been joined by airborne (Pollack et al., 1990), space-based (Bell et al., 1997; Erard et al., 2000), and orbital sensors (Bibring et al., 1989, 2004; Murchie et al., 2002).

Reflectance spectroscopic investigations have provided some of the most important advances in our understanding of Mars geology, such as detecting the presence of various phyllosilicates and hydrated sulfates (Gendrin et al., 2005; Langevin et al., 2005; Poulet et al., 2005), in addition to a number of anhydrous minerals (Mustard et al., 1997; Murchie et al., 2000).

The detection of specific H_2O- and OH-bearing minerals leads to the issue of the robustness of the mineral identifications. This issue includes whether these minerals are expected to be stable at the martian surface, how their spectral properties

* Corresponding author. Fax: +1 (204) 774 4134.
E-mail address: e.cloutis@uwinnipeg.ca (E.A. Cloutis).

0019-1035/$ – see front matter
doi:10.1016/j.icarus.2007.10.028

may change upon exposure to Mars surface conditions, whether they retain characteristic and unique spectral properties, and whether they may be spectrally similar to other minerals. A related question is whether other minerals expected to be present on Mars, or tentatively detected, are stable under current Mars surface conditions, and hence spectrally detectable. These include various carbonates, hydroxides, and organic molecules.

Different investigators have addressed these issues using a variety of approaches, such as thermodynamic modeling (e.g., Gooding, 1978; King et al., 2004; Marion and Kargel, 2005; Navrotsky et al., 2005). Other investigations are laboratory based and involve exposing both synthetic and natural samples to nonambient conditions designed to simulate some aspects of the martian surface, and monitoring their behavior using a variety of techniques, such as electron paramagnetic resonance spectroscopy (Yen et al., 2000), thermogravimetry (Hamad, 1976; Vaniman et al., 2004; Vaniman and Chipera, 2006), X-ray diffraction (Bish et al., 2003; Vaniman et al., 2004; Vaniman and Chipera, 2006; Robertson and Bish, 2007; Xu et al., 2007), Raman spectroscopy (Wang et al., 2006a, 2006b, 2007; Freeman et al., 2007a); reflectance spectroscopy (Bishop and Pieters, 1995; Bonello et al., 2005; Freeman et al., 2007a; Prieto-Ballesteros et al., 2007), and analysis of evolved gases (Mukhin et al., 1996). These studies have shown that the stability of H_2O-bearing minerals, in particular, is sensitive to changes in conditions such as relative humidity, temperature and atmospheric pressure (Bish et al., 2003; Vaniman et al., 2004; Vaniman and Chipera, 2006). Laboratory-based studies can also provide a useful check on thermodynamic models (O'Connor, 1968; Pollack et al., 1970; Huguenin, 1974).

Many of these previous studies have focused on sulfate minerals because of their recent identification on Mars, and the complex stability relations that exist between different members of this group. Many previous laboratory-based studies have required removal of the sample from the environment chamber for analysis, or simulated only a subset of martian surface conditions. The current study was designed to overcome some of these earlier limitations by including a wider range of mineral species, directly monitoring spectral reflectance changes in samples while they are held in a simulated martian surface environment, and exposing the samples to simulated Mars surface conditions of atmospheric composition and pressure, temperature and ultraviolet light regime. The goals of this study are: (1) to determine whether mineral identifications made to date using reflectance spectra of Mars are robust; (2) to assess any spectral changes accompanying exposure to Mars surface conditions for a range of known, presumed or expected Mars minerals; and (3) relate these spectral changes to specific compositional or structural changes.

This study complements the results obtained by other investigators using different analytical techniques and environmental conditions. The picture that is emerging from these studies is that some mineral groups, such as Mg-sulfates (Vaniman et al., 2004), have very complex stability fields, while others, such as Ca-sulfates (Robertson and Bish, 2007), seem to exhibit more well-defined behavior.

2. Experimental procedure

A total of 32 minerals was used in the experimental runs (two minerals were run twice, and one was run at two grain sizes) (Table 1). The samples were ground by hand in an alumina mortar and pestle and dry sieved to obtain the requisite size fractions with two exceptions: the palagonitic soil (PAL101) was dry sieved without crushing, and the Athabasca oil sand (TAR17) was used as a whole-rock sample. Fine-grained (<45 μm) fractions were used whenever possible in order to mimic the fine-grained nature of the uppermost martian surface (Dollfus et al., 1993) and to maximize surface to volume ratios so that any alteration would be more readily observed. To better understand the spectral-compositional-structural relations from the experimental runs, the initial samples were characterized by X-ray diffraction, X-ray fluorescence and wet chemistry. Analytical procedures are described in Mertzman (2000) and Cloutis et al. (2006). The compositions of the samples used in this study are provided in Table 2.

Simulated Mars surface conditions were produced using the University of Winnipeg's mini Mars Environment (mini-ME) chamber (Craig et al., 2001). This chamber can accommodate a 40 mm diameter sample disk, which in our experiment contained 10 sample wells, each one 8 mm in diameter and 6 mm deep. Mars atmospheric composition was approximated using commercial grade CO_2 that was passed through Drierite®. The chamber outlet was connected to a BOC Edwards Model XDS 5C® scroll pump that was run continuously. Constant atmospheric pressure was maintained by balancing inflow and outflow with needle valves. This allowed a constant airflow to remove any evolved H_2O and OH. Atmospheric pressure was monitored using a Teledyne Hastings DV-4® vacuum gauge. For the lower-pressure exposures, the CO_2 inflow was turned off but the scroll pump was kept running. It should be noted that pH_2O in the chamber was not monitored during these experiments.

It was felt that low sample temperatures would likely impede any dehydration that the samples might undergo, necessitating longer duration experiments than was feasible. However, we did attempt to restrict sample temperatures to a maximum close to maximum current surface temperatures on Mars (~20 °C). This was achieved by circulating water into the chamber via a piping system that was in thermal contact with the sample disk. Our experimental setup did not allow direct monitoring of sample temperature, but we were able to monitor the temperature of the walls of the chamber, and this temperature was normally between 10 and 20 °C. Even with an in-chamber temperature-monitoring capability, it is likely that the surface of the sample (which is viewed by the spectrometer) differs from that of the sample holder (Presley and Craddock, 2006). Elevated temperatures (above ambient) at the sample surface would have occurred during UV irradiation. Measurements of sample temperatures during UV irradiation (in atmosphere) showed that the sample surface can be hotter than room temperature. This effect was most significant during the final lowest pressure excursion (1.3 Pa) of run 2 when an unexpected shutdown of our cooling system over a weekend during UV irradiation occurred.

Table 1
Conditions of experimental runs and samples used in each run

Run #	Days at 660 Pa	Days at 660 Pa + UV	Days at few Pa	Days at few Pa + UV	Lowest pressure (Pa)	Sample ID	Sample name	Grain size (μm)
1	14	9	25	0	1.0	CLI101	Clinochlore	<45
						CRB118	Calcite	<45
						CRB118	Calcite	90–180
						NON101	Nontronite	<45
						SPT116	Jarosite	<45
						SPT127	Gypsum	<45
						SPT143	Hexahydrite	<45
						SRP104	Serpentine	<45
2	9	11	9	7[a]	1.3	CHM102	Chamosite	<45
						SPT117	Copiapite	<45
						SPT121	Fibroferrite	<45
						SPT128	Anhydrite	<45
						SPT129	Alunite	<45
						SPT137	Paracoquimbite	<45
						SPT139	Rhomboclase	<45
						SPT141	Kieserite	<45
						SPT144	Szomolnokite	<45
3	9	10	10	0	2.6	BEI101	Beidellite	<45
						BER102	Berthierine	<45
						CRO101	Cronstedtite	<45
						GLA103	Glauconite	<45
						HAL001	Halloysite	<45
						HIS001	Hisingerite	<45
						SAP101	Saponite	<45
						SPT127	Gypsum	<45
						SPT143	Hexahydrite	<45
4	11	10	10	0	2.6	CRB114	Magnesite	<45
						CRB215	Hydromagnesite	<45
						GIL101	Gilsonite	<45
						MON101	Montmorillonite	<45
						PAL101	Palagonitic soil	<45
						OILS10	Oil shale	<45
						OOH003	Goethite	<45
						OOH012	Diaspore	<45
						TAR17	Oil sand	Unsorted

[a] Sample temperatures were below 20 °C in all cases except for the few Pa plus UV irradiation portion of run 2, when a failure of the cooling system results in a 2 day excursion to ∼40 °C.

Chamber temperature was 30 °C before the cooling system was restored. We estimate that sample surface temperatures may have reached as high as 40 °C during this time based on tests of sample heating (in air) by UV irradiation.

The chamber is equipped with a 50 mm diameter, 10 mm-thick sapphire window. This window provides <1% absorbance from 0.2 to 6 μm. The lower-wavelength limits correspond very closely to the lower-transmission limit of the Mars atmosphere (Hord et al., 1970; Kuhn and Atreya, 1979; Cockell et al., 2000; Patel et al., 2004). This allows UV sample irradiation and spectral measurements across the 0.2–6 μm range.

Reflectance spectra over the 0.35–2.5 μm range were acquired with an Analytical Spectral Devices FieldSpec Pro HR® spectrophotometer. The spectral resolution of the instrument varies between 2 and 7 nm and spectral sampling is done at 1.4 nm intervals. The data are internally resampled by the instrument to 1 nm intervals. Spectra were acquired at $i = 0°$ and $e = 0°$ using a bifurcated reflectance probe that contains a randomly arranged mix of 78 illumination and 78 pick-up optical fibers. Illumination was provided by an ASD 11 W quartz–tungsten-halogen light source. A total of 2000 spectra were averaged to improve the signal-to-noise ratio. Reflectance spectra were measured relative to a halon standard located in the sample disk. The spectra were corrected for minor irregularities in halon's absolute reflectance in the 2.0–2.5 μm range by ratioing the halon to a calibrated Spectralon® disk. Wavelength calibration was monitored through regular measurements of an HoO-doped Spectralon® standard. The spot size measured by this instrument was ∼3 mm in diameter; thus the sample or standard filled the field of view of the detector. The bifurcated probe was in direct contact with the sapphire window to minimize reflection from the window's upper surface.

The ASD spectrometer has three detectors that collectively cover the full 0.35–2.5 μm range as follows: 0.35–1.0, 1.0–1.83, and 1.83–2.5 μm. The bifurcated cable used for the measurements has a random arrangement of illumination and pick-up fibers, and each pick-up fiber directs the light to one of the three detectors. As a result, there are often small jumps in the data where the detector changeovers occur (1.00 and 1.83 μm). These jumps were removed by correcting the shortest (0.35–

Table 2
Compositions of the samples used in this study

	Phyllosilicates and palagonitic soil						
Sample name	Beidellite	Berthierine	Chamosite	Clinochlore	Cronstedtite	Glauconite	Halloysite
(wt%)[a]	BEI101	BER102	CHM102	CLI101	CRO101	GLA103	HAL001
NHNM#[b]		93555			193910	46447	
SiO_2	63.59	27.94	21.77	33.78	16.15	60.45	53.18
Al_2O_3	22.74	7.92	5.62	21.63	0.24	9.95	45.46
TiO_2	0.75	0.52	0.23	0.22	0.00	0.26	0.00
Fe_2O_3	5.24	30.59	25.92	4.23	63.51	16.06	0.44
FeO	0.18	20.41	29.09	5.96	15.96	1.51	0.00
MnO	0.02	0.11	0.51	0.20	0.16	0.02	0.01
MgO	2.09	3.42	4.06	32.18	0.22	3.51	0.11
CaO	1.25	4.57	6.36	0.07	0.56	0.95	0.15
Na_2O	1.04	0.28	0.77	0.11	0.72	0.20	0.07
K_2O	2.19	0.05	0.06	0.00	0.00	6.27	0.05
P_2O_5	0.04	1.81	1.71	0.02	0.12	0.14	0.14
Total[c]	99.13	97.62	96.10	98.34	97.64	99.32	99.61
LOI[d]	12.86	6.45	20.87	11.89	8.64	9.53	16.29
XRD[e]	Be, Qt, Ka, Mo, Mu	Br	Ch	Cl	Cr, Ca	Gl, Qt	Am, Ha

	Hisingerite	Montmorillonite	Nontronite	Palagonitic soil	Saponite	Serpentine
	HIS001	MON101	NON101	PAL101[f]	SAP101	SRP104
					C3810	152246
SiO_2	46.36	65.85	61.40	41.24	62.89	44.21
Al_2O_3	5.71	19.89	9.49	25.00	18.76	0.32
TiO_2	0.48	0.67	0.38	3.62	0.90	0.04
Fe_2O_3	30.53	5.65	22.08	12.58	7.29	10.11
FeO	0.00	0.26	0.79	2.77	0.39	1.34
MnO	0.39	0.02	0.03	0.29	0.04	0.08
MgO	9.77	2.02	1.07	3.52	1.85	43.21
CaO	2.00	0.94	0.10	5.11	2.30	0.07
Na_2O	3.17	1.30	0.15	2.74	2.12	0.14
K_2O	0.26	2.90	3.67	0.67	2.69	0.00
P_2O_5	0.08	0.04	0.51	1.34	0.16	0.01
Total[c]	98.75	99.54	99.67	98.88	99.39	99.53
LOI[d]	14.63	10.38	8.56	13.89	12.27	12.21
XRD[e]	Am, Hi	Mo, Qt	No, Qt	Am, Pl	Sp, Pl	Sr
	Mo			Px, Mt		

	Hydroxides		Carbonates		
	Goethite	Diaspore	Magnesite	Calcite	Hydromagnesite
	OOH003	OOH012	CRB114	CRB118	CRB215
SiO_2	1.40	0.28	31.21	0.97	1.24
Al_2O_3	1.22	81.22	0.00	0.05	0.10
TiO_2	0.07	0.15	0.00	0.00	0.01
Fe_2O_3			0.00	0.11	
FeO			0.00	0.00	
Fe_2O_3[g]	89.29	0.62			0.18
MnO	0.21	0.01	0.01	0.00	0.01
MgO	0.19	0.04	53.79	1.90	73.43
CaO	0.06	0.90	14.63	97.03	0.53
Na_2O	0.48	1.10	0.02	0.22	0.00
K_2O			0.00	0.00	0.04
P_2O_5			0.04	0.00	0.04
LOI	9.8[h]	14.3[h]	34.57[d]	43.07[d]	47.89[d]
Total	102.72	98.62	99.70[c]	100.28[c]	75.58[c]
XRD[e]			Mg, Hu	Ca	Hm, Mg

(*continued on next page*)

1.0 μm) and longest (1.83–2.5 μm) intervals to the middle interval (1.0–1.83 μm), which is thermoelectrically cooled and temperature controlled.

Reflectance spectra over the 2–6 μm range were measured using a Designs and Prototypes Model 102F® Fourier-transform infrared spectrometer. Sample illumination was provided by an in-house 50 W quartz–tungsten-halogen illumination source directly illuminating the sample through an open-air aluminum light pipe. This allows a wide wavelength range of light (from the filament and heated envelope of the bulb) to il-

Table 2 (*continued*)

	Sulfates					
Sample name (wt%)[a]	Jarosite SPT116	Copiapite SPT117	Fibroferrite SPT121	Gypsum SPT127	Anhydrite SPT128	Alunite SPT129
SiO_2	0.05	13.86	2.60	0.00	0.00	0.00
Al_2O_3	0.11	8.28	0.21	0.20	0.15	74.51
TiO_2	0.02	0.16	0.04	0.00	0.00	0.00
Fe_2O_3	82.52	66.94	95.02	0.03	0.04	0.00
FeO	0.29	0.00	0.00	0.00	0.00	0.05
MnO	0.01	0.21	0.04	0.00	0.00	0.00
MgO	0.17	8.47	0.31	0.07	0.06	0.07
CaO	0.17	0.47	0.70	32.46	46.06	0.12
Na_2O	4.77	0.79	0.58	0.30	0.78	0.46
K_2O	10.38	0.43	0.10	0.00	0.00	23.54
P_2O_5	0.91	0.08	0.03	0.01	0.02	0.76
SO_3	32.50	39.95	35.38	46.55	37.38	35.88
Total[i]	99.40	99.69	99.63	100.20[j]	100.38[j]	99.51
LOI[d]	35.46	66.85	63.22	20.58	15.89	40.15
XRD[e]	Ja	Co, Ko	Fi, Bu	Gy	An, Gy	Al

	Paracoquimbite SPT137	Rhomboclase SPT139	Kieserite SPT141	Hexahydrite SPT143	Szomolnokite SPT144
SiO_2	0.03		0.00	0.00	31.42
Al_2O_3	3.37		0.02	0.06	10.77
TiO_2	0.10		0.00	0.00	0.98
Fe_2O_3	33.12		0.48	0.00	17.48
FeO	0.00		0.00	0.00	8.88
MnO	0.00		0.01	0.01	0.03
MgO	0.18		15.38	25.09	1.99
CaO	0.06		0.06	0.46	1.48
Na_2O	0.62		13.82	0.94	0.66
K_2O	0.04		4.04	0.09	1.28
P_2O_5	0.04		0.02	0.04	0.11
SO_3	25.44				23.53
Total[k]	109.23		80.38	64.80	104.63
LOI[d]	71.67	74.66	46.55	38.11	29.55
XRD[e]	Pc, Ko	Rh	Ki, Hl	Hx, Am	Sz, Rz Py, Ka

Source of samples: BEI101: near Cameron, Coconico Co., AZ, USA; BER102: France; CLI101: near Murphys, Calaveras Co., CA, USA; CRO101: 411 level, Llallagua, Bolivia; GLA103: Villers-sur-Mer, Calvados, France; HAL001: Tintic district, UT, USA; SPT116: Copiapa Jarosite Mine, Dona Ana Co., NM, USA; SPT117: Alma Pyrite Mine, Leona Heights, Oakland, Alameda Co., CA, USA; SPT121: Skouriatissa, Cyprus; SPT127: UT, USA; SPT128: unknown locality; SPT129: Marysvale, Piute Co., UT, USA; SPT137: Coso Hot Spring, Inyo Co., CA, USA; SPT139: Alcaparrosa, Chile; SPT141: Stassfurt, Saxony, Germany; SPT143: Basque Lakes, near Ashcroft, BC, Canada; SPT144: Getchell Mine, near Golconda, Humboldt Co., NV, USA.

[a] wt% of elements expressed as oxides.

[b] Smithsonian Institution National Museum of Natural History sample number.

[c] Total expressed on a volatile-free basis.

[d] Weight loss upon heating sample in air from room temperature to 950 °C for 1 h.

[e] Phases identified in sample by X-ray diffraction (in order of abundance). Abbreviations—Am: amorphous component; Be: beidellite; Br: berthierine; Ca: cassiterite; Ch: chamosite; Cl: clinochlore; Cr: cronstedtite; Gl: glauconite; Ha: halloysite; Ka: kaolinite; Mo: montmorillonite; Mu: muscovite; Qt: quartz; Hi: hisingerite; Mo: montmorillonite; Mt: magnetite; Qt: quartz; No: nontronite; Pl: plagioclase feldspar; Px: pyroxene; Sp: saponite; Sr: serpentine; Ca: calcite; Hm: hydromagnesite; Hu: huntite; Mg: magnesite; Al: alunite; An: anhydrite; Bu: butlerite; Fi: fibroferrite; Gy: gypsum; Ja: jarosite; Co: copiapite; Ko: kornelite; Hl: halite; Hx: hexahydrite; Ka: kaolinite; Ki: kieserite; Ko: kornelite; Pc: paracoquimbite; Py: pyrite; Rh: rhomboclase; Rz: rozenite; Sz: szomolnokite.

[f] Sample HWMK600 (Morris et al., 2000); analytical data for 5–53 μm fraction.

[g] All Fe reported as Fe_2O_3.

[h] Weight loss upon heating sample in air from room temperature to 1000 °C.

[i] Total expressed on a volatile (LOI- and SO_3-free basis).

[j] Total includes loss on ignition and SO_3.

[k] Total includes loss on ignition.

luminate the sample. The light was directed at the sample at an angle of 35° from normal. The FTIR spectrometer is equipped with a Designs and Prototypes customized optical assembly that allows a spot size of ∼7 mm to be viewed by the instrument; all measurements were made at normal incidence ($i = 0°$). Reflectance spectra were acquired relative to a 35 mm diameter Infragold® diffuse gold-coated standard. The standard was illuminated and viewed with the same geometry as the samples. The gold standard was located external to the chamber and was viewed through an identical sapphire window as that used on the environment chamber. The chamber has a 1 mm path length between the surface of the sample and the bottom of the

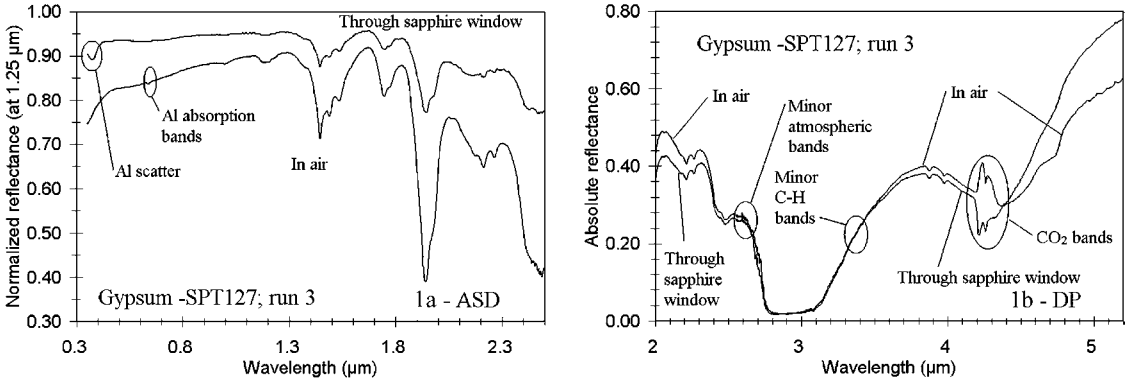

Fig. 1. Reflectance spectra of gypsum showing changes in spectral features for samples measured through a sapphire window and in air. (a) 0.35–2.5 μm spectra acquired with ASD spectrometer; (b) 2.0–5.2 μm spectra acquired with D&P spectrometer.

sapphire window. This same spacing was used for the gold standard. However, this 1 mm path is through low-pressure CO_2 in the case of the samples and ambient air in the case of the gold standard. This difference resulted in the appearance of CO_2-related features in the 4.2–4.4 μm region.

The resulting spectra exhibited some spurious features that we were able to trace to specific causes in most cases. As mentioned, differences in the composition of the atmosphere between the samples and gold standard led to CO_2-related features in the 4.2–4.4 μm region. The sapphire windows used for the environment chamber (and gold standard) did not have any antireflection coatings, as we felt that this could lead to the introduction of unwanted spectral features. As a result, reflections from the surfaces of the sapphire windows were quite noticeable. The light scattered by the sapphire window also interacted with the interior of mini-ME. This was seen as a bright diffuse light in the chamber, even though the incident light could be directed to a spot size of ∼10 mm (with additional weaker diffraction rings). Spectral measurements of the aluminum sample holder showed that it exhibited slope changes shortward of ∼0.55 μm, as well as some minor absorption bands between 0.62 and 0.65 μm; the aluminum environment chamber walls also contributed to these features. These features are evident in many of the ASD reflectance spectra and arise from the fact that the sample and standard are located in different parts of the sample disk and hence will be differentially affected by scattered light in the environment chamber. However, our interest is focused on the relative spectral changes in absorption band depths and positions rather than any absolute changes, and hence these spurious features do not critically impede spectral analysis. The anodized aluminum holder used to keep the sapphire window in place contributed some small C–H absorption features between 3.35 and 3.5 μm in some of the spectra, again due to light scattered in the chamber. An additional effect that arose in some of the spectra over the course of the experimental runs was a change in overall slope. This effect was likely due to a greater contribution from the walls of the aluminum sample wells, as a number of the samples “shrank” in their holders over the course of the run. Our aluminum sample holder is known to have a red sloped spectrum, and as the surface of a powdered sample moves down during self-compression or dehydration, there will be a greater contribution from the aluminum sample holder walls. Consequently, our analysis focused largely on changes in absorption band depths and positions versus overall slopes.

One additional feature that was seen in the reflectance spectra due to the scattered light was a loss of contrast and a general increase in overall reflectance, a characteristic we term “white noise.” This caused mineral absorption bands to be shallower in the chamber spectra than in the spectra of the same minerals acquired outside the chamber. Fig. 1 shows an example of the loss of contrast as well as some of the spurious features identified in the spectra.

In the course of the experimental runs, many of the samples exhibited a decrease in volume that manifested itself variously as the sample surface dropping down, the sample moving away from the sides of the well, or cracking. When coupled with the small path length of the ASD probe to the sample, the drop in sample surface sometimes resulted in a significant change in overall reflectance. This also caused a change in path length, introducing additional atmospheric absorption bands in the 2.5–2.7 μm region. As the samples could not be accessed during the experimental run, it was decided to analyze the results as scaled reflectance (all spectra normalized to unity at 1.25 μm), rather than in absolute reflectance. The working distance of the FTIR spectrometer is approximately 5 cm from the top of the sapphire window. As a result, small changes in the height of the sample surface did not have as great an effect on overall reflectance. Consequently, the FTIR spectra are presented in absolute rather than normalized reflectance. Changes in the height of the sample surface would however lead to some changes in how light was scattered within the chamber for different dates, and this likely accounts for some of the changes in overall reflectance seen in the FTIR spectra.

Spectral analysis involved measuring wavelength positions of absorption bands and band depths. Band depths were calculated by constructing a straight line continuum on either side of a feature of interest and measuring the depth as per Eq. (32) of Clark and Roush (1984).

The experimental runs were designed to address a number of specific issues related to the stability of different minerals under martian surface conditions, including stability as a function of structure, OH versus H_2O, the relative importance of atmospheric pressure versus ultraviolet irradiation, and the effects

of excursions to lower atmospheric pressure. The experimental conditions varied somewhat from run to run due to scheduling issues and instrumental performance.

The general experimental sequence for each run was as follows: the samples were initially exposed to 660 Pa CO_2 (5 Torr; 0.0065 atm) (equivalent to Mars surface pressure), followed by the addition of UV irradiation (while maintaining the 660 Pa CO_2 atmosphere), followed by exposure of the samples to pressures of between 1.0 and 2.6 Pa (8–20 Torr) CO_2 without UV irradiation (the lower limit determined by the efficiency of the scroll pump during a particular run). In run 2, the lowest pressure exposure was followed by the addition of UV irradiation. The experimental conditions for each run are summarized in Table 1.

The purpose of the low pressure (1.0–2.6 Pa) exposure was to see whether this would accelerate any changes in the spectra that were occurring during the 660 Pa exposure, as well as to determine whether low pressure exposure would lead to different spectral changes than those seen at 660 Pa. The hope was that short periods of exposure of samples to a few Pa pressure might simulate longer duration exposures at 660 Pa. However, there are many factors that control mineral stability (e.g., Hamad, 1976) and hence our results may only be suggestive of long term mineral stability at 660 Pa.

UV irradiation was done using two 25 W deuterium lamps. The output of the lamps was directed by a free-air light pipe of the same diameter as the sample holder onto the samples through the sapphire window. The intensity of the incident UV radiation was determined to be one day of laboratory irradiation being equivalent to approximately one decade on Mars.

3. Results

The minerals that were selected for this study were based on a number of criteria, including whether they had been tentatively or positively identified on Mars to date, or were plausible candidates for the Mars surface. We also emphasized samples that are OH- and/or H_2O-bearing, as anhydrous minerals are not expected to exhibit significant spectral changes, with the possible exception of changes in oxidation state of various transition series elements. In the ensuing discussion, the various samples are divided into compositional groups and further subdivided, where appropriate, into common subgroups, largely on the basis of their volatile contents, e.g., H_2O versus OH.

In this study, we use the term “stable” to mean that no measurable and systematic changes in absorption band wavelength positions or depths were observed over the course of the experiment. This does not mean that such minerals are stable over geological time scales, and other experimental approaches are more sensitive to minor compositional changes that would not be reflected in spectroscopic examinations (e.g., Mukhin et al., 1996). Nevertheless, this study is useful for identifying minerals that undergo rapid decomposition, as well as for assessing relative instability.

A variety of phyllosilicates were included in this study because a number of them have been detected on Mars. Species tentatively detected to date include serpentine (Mustard et al., 2007), montmorillonite (Poulet et al., 2005; Mustard et al., 2007), nontronite (Poulet et al., 2005; Mustard et al., 2007), saponite (Mustard et al., 2007), chlorite (clinochlore) (Mustard et al., 2007), chamosite (Poulet et al., 2005), illite (Mustard et al., 2007), and kaolinite (Mustard et al., 2007). These minerals include representatives from most of the major structural groups and include species that normally possess interlayer H_2O (montmorillonite, nontronite, saponite). The phyllosilicates are divided into structural groups based on the arrangement of octahedrally-coordinated layers (O) and tetrahedral (T) layers and the nature of interlayer cations (H_2O versus other cations).

3.1. T–O phyllosilicates—Serpentine, cronstedtite, berthierine, halloysite

Phyllosilicates of the T–O group consist of a single tetrahedral and octahedral layer joined together by sharing oxygens, and have a 7 Å layer thickness. This group can be further subdivided into dioctahedral and trioctahedral species based on whether the octahedrally-coordinated sites are fully occupied by divalent cations (trioctahedral) or if only two thirds are occupied by trivalent cations (dioctahedral). Serpentine and cronstedtite are trioctahedral, while berthierine and halloysite are dioctahedral. These species do not contain interlayer H_2O as an integral part of their structure, with the exception of halloysite. Serpentine is the only member of this group tentatively identified on Mars to date (Mustard et al., 2007).

3.1.1. Serpentine (T–O trioctahedral)

The results of the experimental run for serpentine (SRP104) are shown in Fig. 2a. Its ideal formula is $A_3Si_2O_5(OH)_4$, where A is Mg, Fe^{2+}, Ni; Mg is by far the most common cation. Serpentine spectra are normally characterized by a series of up to four partly overlapping OH-stretching overtones in the 1.38–1.42 μm region, and an Mg–OH absorption feature near 2.31 μm that is due to combinations of an OH stretch and an Mg–OH bend (Clark et al., 1990); the double-band nature of the feature near 2.31 μm (Bishop et al., 2002) is seen in our spectra. The cause of the absorption feature near 2.1 μm is uncertain, but is also likely due to an Al–OH combination band (King and Clark, 1989). Weaker bands are often present in the 2.38–2.44 μm region, also likely due to metal–OH combinations. The presence of Fe can lead to absorption bands near 0.7 μm due to Fe^{2+}–Fe^{3+} intervalence charge transfer and near 1 μm due to either Fe^{2+} crystal field transitions (two absorption bands near 0.9 and 1.1 μm) or Fe^{3+} ligand-field transitions (single absorption near 0.9 μm) (Sherman and Vergo, 1988). Our sample contains both Fe^{3+} and Fe^{2+} (Table 2) which gives rise to the broad absorption feature near 0.7 μm; this feature also reduces the apparent intensity of the expected longer-wavelength Fe^{2+} and Fe^{3+} absorption bands. An expected Fe^{2+} absorption near 1 μm is weak, likely due to the small amount of Fe^{2+} in our sample and the aforementioned spectral overlap. All of the expected Mg–OH combinations and OH-stretching fundamentals and overtones are present. Fundamental stretching bands due to

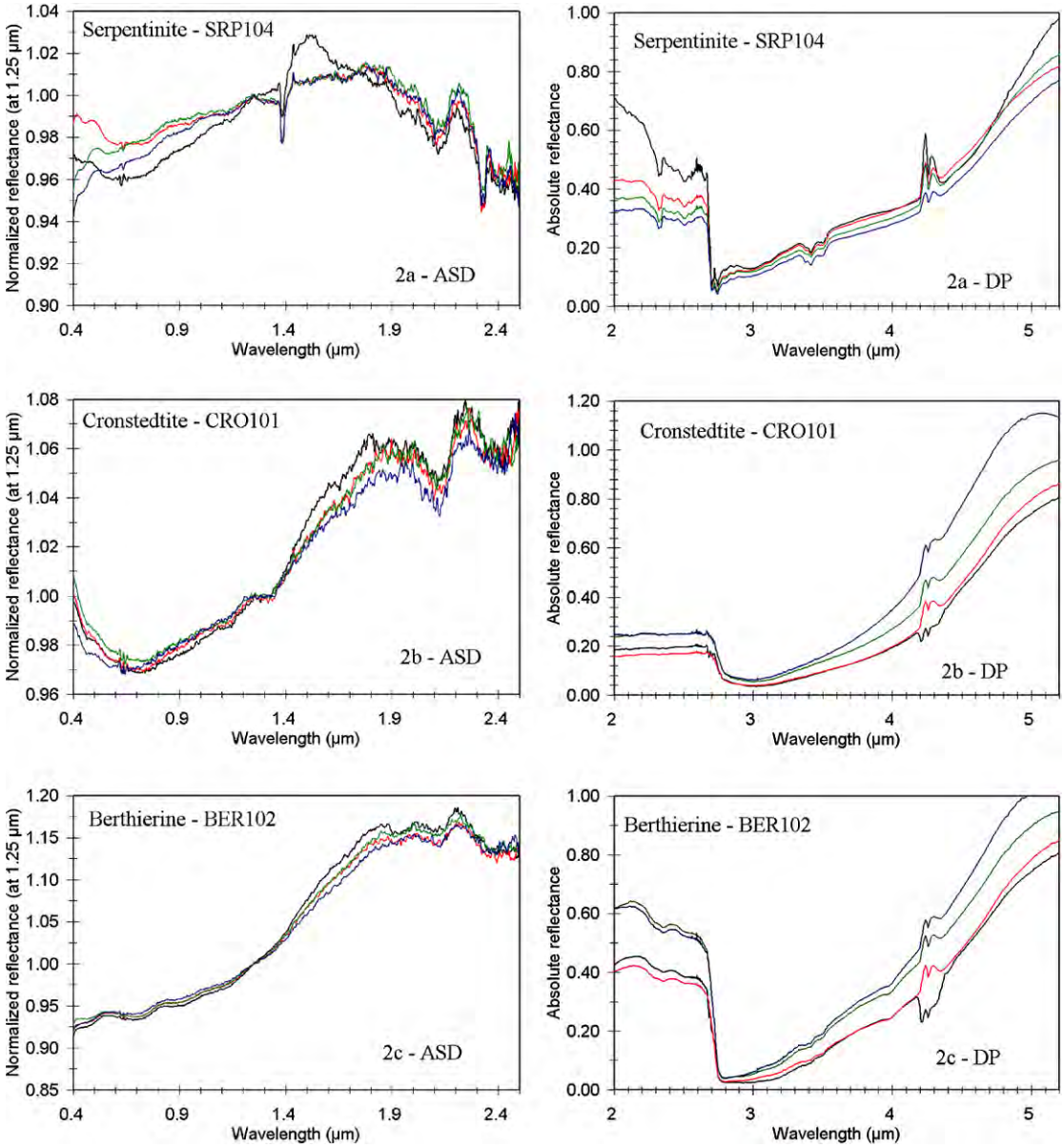

Fig. 2. Reflectance spectra of <45 µm fractions of phyllosilicates and a palagonitic soil acquired over the course of exposure of the samples to simulated Mars surface conditions. Left spectra acquired with ASD spectrometer (ASD); right spectra acquired with D&P spectrometer (DP). (a) Serpentine (SRP104); (b) cronstedtite (CRO101); (c) berthierine (BER102); (d) halloysite (HAL001); (e) beidellite (BEI101); (f) montmorillonite (MON101); (g) nontronite (NON101); (h) saponite (SAP101); (i) glauconite (GLA103); (j) clinochlore (CLI101); (k) chamosite; (CHM102); (l) hisingerite (HIS001); (m) palagonitic soil (PAL101). The distribution of the samples among the experimental runs and run conditions are provided in Table 1. Compositions of the samples are given in Table 2. The curves are color-coded as follows: black: start of experimental run—atmospheric pressure; red: end of 660 Pa exposure; green: end of 660 Pa + UV irradiation exposure; blue: end of few Pa exposure; brown: end of few Pa + UV irradiation exposure (run 2 only).

OH are present between 2.710 and 2.715 µm and between 2.738 and 2.744 µm (Bishop et al., 2002).

Over the course of the experimental run, the most significant change is a gradual decrease in overall reflectance, likely due to shrinkage of the sample. The depths and positions of the various absorption bands do not seem to be affected over the course of the run, and the only measurable change is a decrease in the depth of the adsorbed-H_2O band near 3 µm. The significant difference in overall spectral shape between the first spectral measurement and subsequent measurements likely relates to early compaction of the sample when low-pressure conditions were first applied.

As noted, our experiment included exposure of the samples to Mars pressures (660 Pa) as well as much lower pressures (a few Pa) and UV irradiation. It seems that with the exception of the loss of adsorbed H_2O, serpentine is quite stable and its characteristic absorption features are not appreciably affected by exposure to Mars surface conditions.

3.1.2. Cronstedtite (T–O trioctahedral)

Cronstedtite (CRO101) has an ideal formula Fe_2^{2+} Fe^{3+}-$(SiFe^{3+})O_5(OH)_4$, and is essentially an Fe-rich version of serpentine, with some additional substitution of Fe^{3+} for Si^{4+}. The higher Fe content results in low overall reflectance (Fig. 2b)

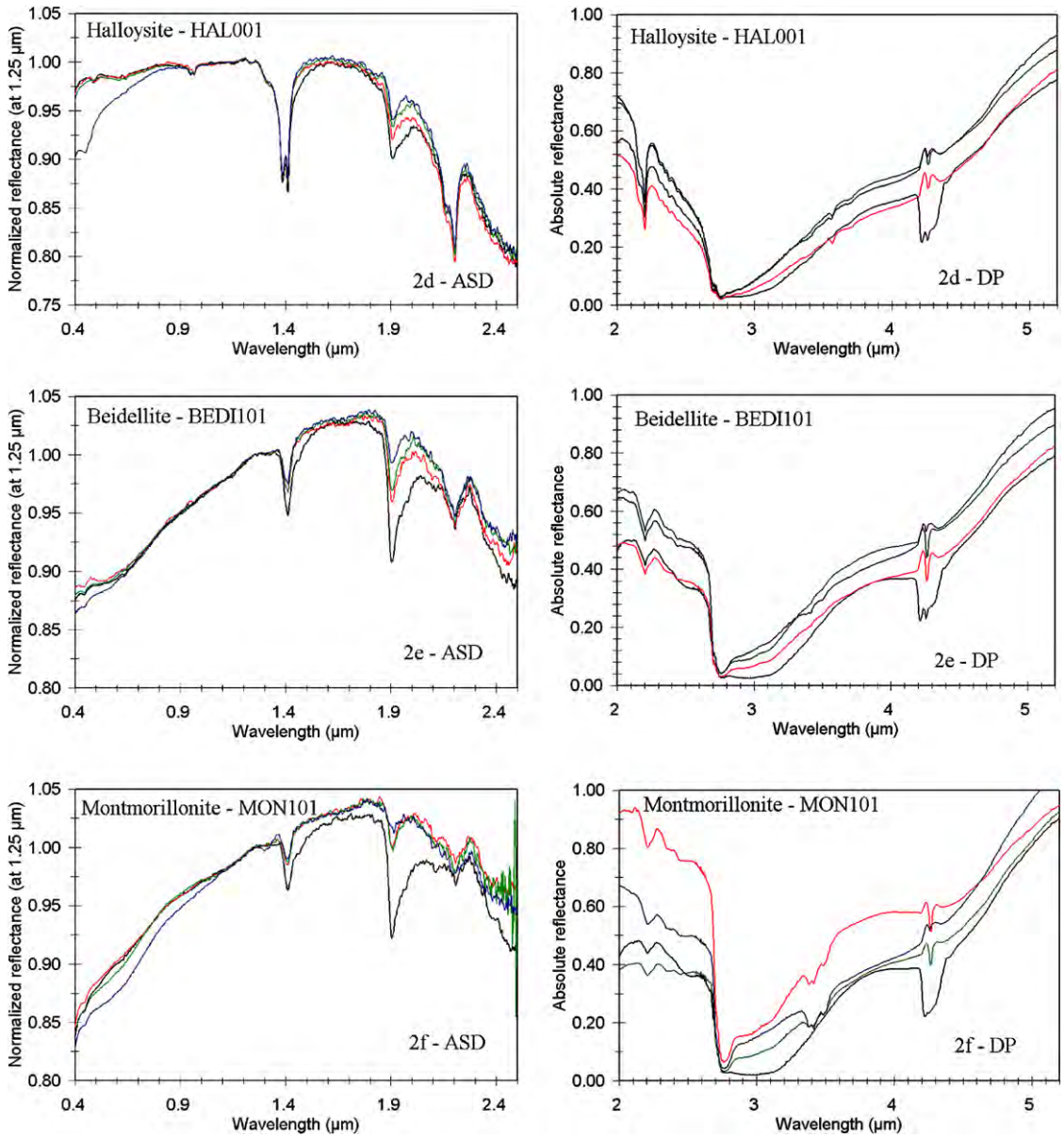

Fig. 2. (*continued*)

and broader Fe-related absorption bands below ~1.2 µm. Our spectrum is similar to a cronstedtite spectrum measured by Calvin and King (1997). The Fe^{2+}–Fe^{3+} charge transfer band is apparent near 0.7 µm and this feature dominates the lower-wavelength region. Expected Fe^{3+} and Fe^{2+} absorption bands in the 0.9–1.1 µm region are not well-resolved due to the low overall reflectance and broadness of the charge-transfer band. The low overall reflectance also results in a subdued OH stretching overtone in the 1.4 µm region. The low Mg content (Table 2) results in an indistinguishable MgOH band near 2.31 µm. However, the band at 2.11 µm is evident, and this feature was also seen in the serpentine spectrum, suggesting that it is attributable to Fe–OH rather than Mg–OH (Clark et al., 1990). Similarly, the band near 2.4 µm is likely attributable to Fe–OH. At longer wavelengths, well-defined OH stretching vibrations are not seen in the 2.7–2.8 µm region, suggesting either a less well-ordered structure or that the bands are suppressed due to the low overall reflectance. As was the case for serpentine, there are no apparent changes in the wavelength positions or intensities of any of the diagnostic absorption bands over the course of the experimental run. There does seem to be a change in overall slope longward of 3 µm, likely due to a loss of adsorbed H_2O.

3.1.3. *Berthierine (T–O dioctahedral)*

Berthierine (BER102) has an ideal formula of $(Fe^{2+},Fe^{3+},Mg)_{2-3}(Si,Al)_2O_5(OH)_4$. Our analysis indicates that our sample is poorly crystalline and Fe-rich (Table 2). It shows more well-defined Fe-related absorption features than cronstedtite, including an Fe^{2+}–Fe^{3+} charge transfer band near 0.7 µm, an Fe^{3+} band near 0.9 µm and likely Fe^{2+} crystal-field transition bands near 0.9 and 1.1 µm (Calvin and King, 1997) (Fig. 2c). The low overall reflectance suppresses any OH-overtone band

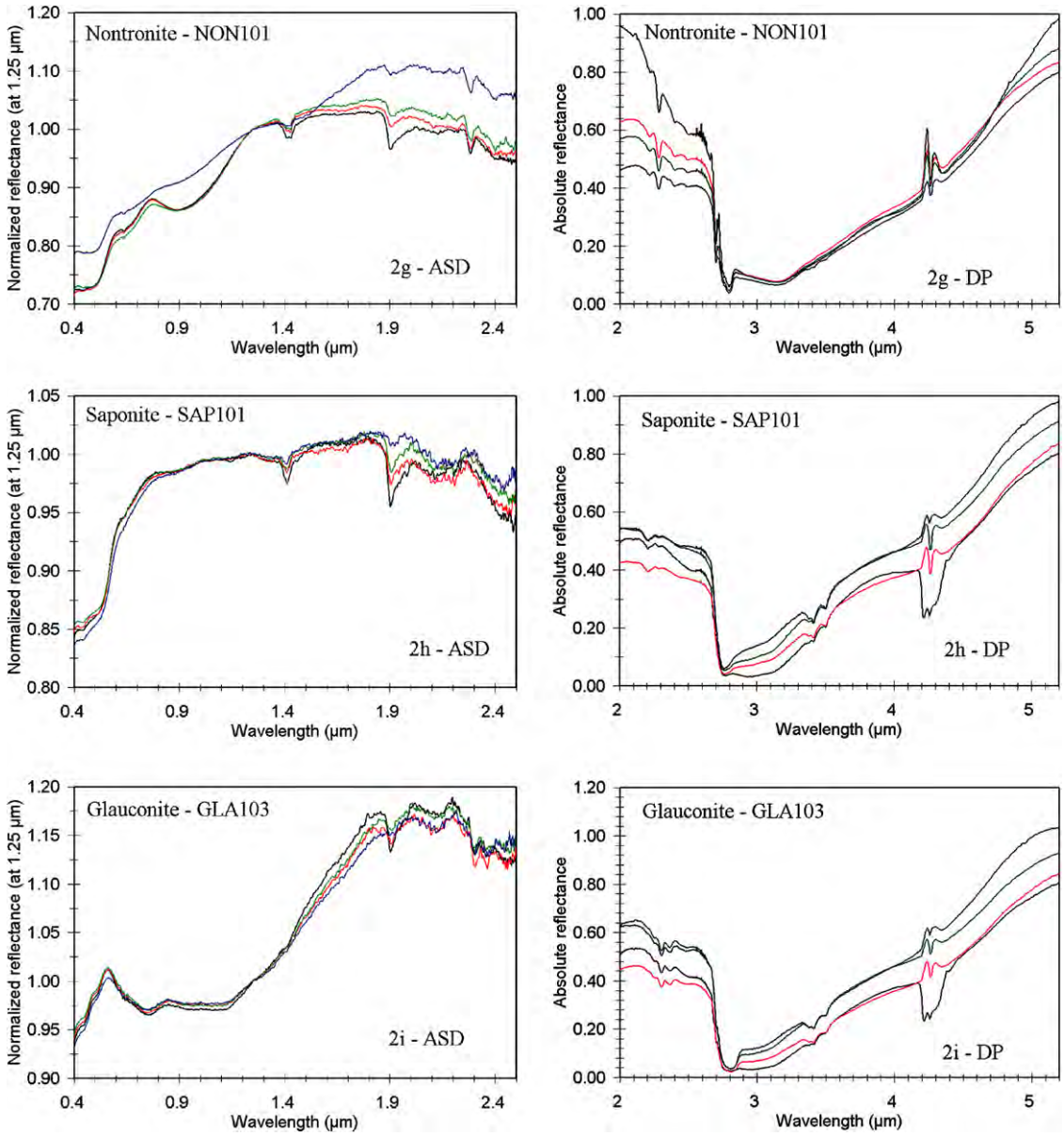

Fig. 2. (*continued*)

in the 1.4 µm region. The weak bands near 2.11 and 2.4 µm are similar to those seen in the cronstedtite and are again attributed to Fe–OH combinations. Individual OH fundamentals in the 2.7–2.8 µm region are not resolved. In the course of the experimental run, no changes are evident in the positions or intensities of the Fe-related absorption features, and the only systematic change is a slight reduction in the intensity of the adsorbed-H_2O feature in the 3-µm region.

3.1.4. Halloysite (T–O dioctahedral)

Halloysite (HAL001) has an ideal formula $Al_2Si_2O_5(OH)_4$. Interlayer H_2O can be accommodated in this mineral, but is not an essential component. Our halloysite sample is compositionally close to the ideal formula (Table 2) and spectrally similar to other H_2O-poor halloysites (Hunt et al., 1973). XRD analysis indicated some degree of noncrystallinity or the presence of an additional poorly crystalline or amorphous component. Compositionally, halloysite is identical to kaolinite but with a different structure. Kaolinite and halloysite are spectrally quite similar, and high-resolution spectra are required to distinguish doublets versus triplets in the 1.4 and 2.2 µm regions of these minerals (Clark et al., 1990).

The high overall reflectance of the sample allows the second-order overtone of the fundamental OH-stretching vibration to be seen near 0.95 µm, in addition to the stronger first-order overtones near 1.4 µm (Fig. 2d). At least two fundamental OH bands are seen near 2.7 and 2.75 µm. The feature near 2.2 µm is attributed to Al–OH combinations, and is also seen in kaolinite spectra. The feature near 1.9 µm is due to adsorbed H_2O or weakly bound interlayer H_2O.

Upon exposure to Mars surface conditions, the only significant spectral changes involve the H_2O-associated absorption bands. The 1.9 µm region feature shows a gradual reduction in intensity from 5.6 to 3.5%, while the 3-µm region feature

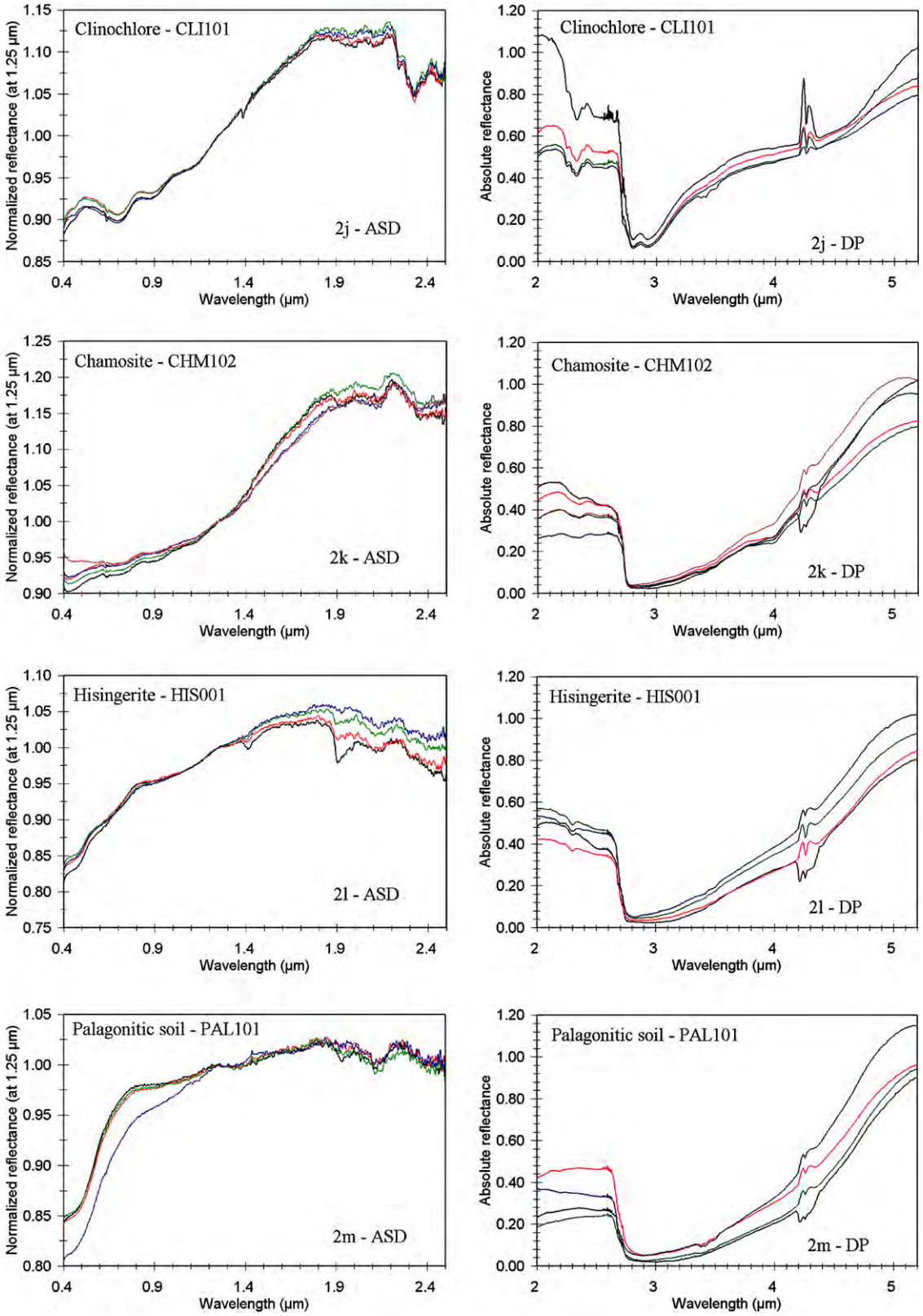

Fig. 2. (*continued*)

becomes more red-sloped as H_2O is lost from the sample. It does not seem that the addition of UV irradiation accelerates the dehydration process or leads to any other spectral changes. The cause of the downturn below 0.9 µm in the last spectrum is likely due to enhanced spectral contributions from the walls of the sample well.

3.2. T–O–T phyllosilicates—Beidellite, montmorillonite, nontronite, saponite

This group involves a T–O–T stacking of tetrahedral and octahedral layers, with or without H_2O between successive T–O–T sequences. The samples from this group all contain interlayer H_2O and include dioctahedral (beidellite, montmorillonite, nontronite) and trioctahedral (saponite) members. These are all smectite clays, whose structures can readily expand or contract to accommodate interlayer H_2O. Beidellite and montmorillonite differ mainly in the cations that can occupy the tetrahedral layers (Si in montmorillonite, Si and a small amount of Al in beidellite) and the octahedral layers (Al and Mg in montmorillonite, Al in beidellite). Our montmorillonite sample (MON101) contains more Si and less Al than the beidellite samples (BEI101), as expected. Montmorillonite, nontronite, and saponite are the three members of this group tentatively identified on Mars (Poulet et al., 2005; Mustard et al., 2007) and included in this study.

3.2.1. Beidellite (T–O–T dioctahedral)

Beidellite (BEI101) has an ideal formula $(Na,Ca_{0.5})_{0.3}Al_2(Si,Al)_4O_{10}(OH)_2{\cdot}nH_2O$. Spectrally, it shows many similarities to montmorillonite, largely due to structural and compositional similarities (Fig. 2e). The presence of H_2O gives rise to an absorption feature near 1.90 μm, and a stretching overtone near 1.46 μm. OH leads to fundamental stretches between 2.70 and 2.75 μm (similar in position to the features seen in the serpentine spectra), and AlAlOH overtones near 1.41 μm. AlAlOH combinations account for the band at 2.20 μm (Post and Noble, 1993). The presence of Fe is not integral to beidellite; the Fe from the analysis is likely due to a small amount of an accessory iron oxide/hydroxide phase and accounts for the reflectance decrease shortward of 1.3 μm. Upon exposure to low atmospheric pressure, the 1.9 μm band shows a progressive decrease in intensity as interlayer H_2O is liberated, decreasing from 10.2% at the start of the run to 3.6% at the end of the run. The 1.46 μm H_2O shoulder also exhibits a rapid decrease in intensity and is essentially unresolvable by the end of the run. The 1.41 μm OH feature exhibits an initial decrease in intensity, but whether this is due to the loss of the adjacent 1.46 μm H_2O feature or due to actual liberation of OH is unclear (band intensity at 1.41 μm decreases from 6.0 to 3.7% over the course of the run). It seems likely that OH is not being liberated from the beidellite because the Al–OH band at 2.20 μm does not exhibit a measurable change in intensity. Complicating the analysis is the fact that our sample contains small, but not well constrained, amounts of kaolinite, montmorillonite, and mica (from XRD analysis). The 3 μm region fundamental H_2O band exhibits a large decrease in intensity which manifests itself as a gradual steepening of the long wavelength wing of the OH fundamental bands in the 2.70–2.75 μm region.

3.2.2. Montmorillonite (T–O–T dioctahedral)

Montmorillonite has an ideal formula $(Na,Ca_{0.5})_{0.7}(Al,Mg,Fe)_4((Si,Al)_8O_{20})(OH)_4{\cdot}nH_2O$, similar to that of beidellite. Our sample (MON101) contains some Fe (Table 2) that is likely present in an accessory iron oxide/hydroxide phase and accounts for the decrease in reflectance shortward of 1.3 μm, similar to the beidellite spectrum. The spectral behavior of montmorillonite largely parallels that of beidellite: rapid decrease in intensity of H_2O-associated absorption bands [at 1.9 (from 9.1 to 1.4%) and 3 μm], a smaller relative decrease in the intensity of the 1.41 μm OH band (from 4.3 to 2.6%) and no change of the 2.2 μm AlAlOH band (Fig. 2f). The intensity reduction in the 1.41 μm OH band but not in the 2.2 μm Al–OH band may be attributable to the loss of OH from a poorly crystalline component; XRD analysis of our sample showed the presence of an amorphous or poorly crystalline component. However, in spite of these apparent losses of OH, the diagnostic OH bands are still detectable and do not show changes in wavelength.

The fact that absorption bands associated with interlayer H_2O do not completely disappear over the course of the experimental run is consistent with the results of Bish et al. (2003) who indicate that smectites (montmorillonite) would remain hydrated under current martian surface conditions, and Bishop and Pieters (1995) who showed that the 1.9 μm H_2O feature persists under martian surface pressures.

3.2.3. Nontronite (T–O–T dioctahedral)

Nontronite (NON101) is an Fe-bearing analogue of montmorillonite with an ideal formula $Na_{0.3}Fe^{3+}_2(Si,Al)_4O_{10}(OH)_2{\cdot}nH_2O$. Spectrally, it has only a superficial resemblance to montmorillonite. The presence of abundant Fe^{3+} (Table 2) results in a broad Fe^{3+}–O charge-transfer feature shortward of ∼0.5 μm and the spin forbidden crystal field transition band near 0.9 μm (Sherman and Vergo, 1988; Fig. 2g). The 1.4 μm region shows two OH-related stretching overtone bands, and the feature at 2.29 μm is likely due to an Fe–OH combination band (Post and Noble, 1993; Clark et al., 1990; Bishop et al., 1997). The 1.9 μm band is attributable to an H_2O bending and stretching combination. Two OH-stretching fundamentals are clearly seen at 2.70 and 2.80 μm; the former is likely due to accessory phases (Bishop et al., 2002).

Upon exposure to Mars surface conditions (660 Pa and 660 Pa plus UV irradiation), few changes are seen except for a gradual decrease in intensity of the 1.9 μm H_2O band; depths of the 1.4 and 2.3 μm OH bands are unchanged. However, upon exposure to 1 Torr pressure, the Fe^{3+} band near 0.9 μm becomes much less prominent, the 1.4 μm OH bands become less intense, and overall slope becomes redder. The latter effect is likely due to a greater contribution from the walls of the sample well and this may contribute to the apparent change in the Fe-associated bands in the 1 μm region. If the changes in the Fe-associated bands are real, two possibilities suggest themselves to explain the change in the Fe^{3+} band. The first is that Fe^{3+} is reduced to Fe^{2+}. The expected Fe^{2+} band near 1 μm becomes more pronounced in the final spectrum as the 0.9 μm band is reduced in intensity. The second (and more likely) possibility is that some OH is liberated from the nontronite, presumably in combination with some sort of structural rearrangement. The evidence for OH loss and structural rearrangement is the fact that the OH-absorption feature in the 1.4 μm region decreases in intensity (from 2.8 to 1.1%) while the absorption band near

2.8 μm changes from a double-band structure, with bands at 2.799 and 2.807 μm, to a single-band structure centered at 2.797 μm. Arguing against this is the fact that the depth of the 2.3 μm OH band is unchanged. The change in the 2.8 μm region is similar to that seen in heat-treated nontronite and is attributed to the removal of FeFeOH groups (Madejová et al., 1996; Karakassides et al., 2000). Removal or disruption of FeFeOH complexes would destroy the hydroxo-bridging necessary for the 0.9 μm band (Sherman, 1985; Sherman and Vergo, 1988). The 0.9 μm Fe^{3+} band is a spin-forbidden band that becomes allowed when adjacent Fe^{3+} cations are O- or OH-bridged (Sherman, 1985). It seems likely that a partial loss of OH, which likely occurs at the lower pressures, disrupts the OH-bridged structure. The fact that the 2.29 μm band, attributable to Fe–OH combinations, is not appreciably reduced in intensity argues for disruption of OH-bridging rather than OH loss as the main mechanism. Thus it seems likely that some combination of OH liberation and structural rearrangement occurs at the lower pressure. However, self-compression of the sample, and hence a greater spectral contribution from the aluminum sample holder cannot be ruled out.

3.2.4. Saponite (T–O–T trioctahedral)

Saponite (SAP101) has an ideal formula $(Ca/2,Na)_{0.3}(Mg,Fe^{2+})_3(Si,Al)_4O_{10}(OH)_2{\cdot}4H_2O$. Our sample also contains Fe^{3+}, but less than is present in our nontronite sample (Table 2). Spectrally, it exhibits the strong decrease in reflectance below ~0.6 μm, attributable to Fe^{3+}-O charge transfer (Fig. 2h). The presumed lack of OH-bridged Fe^{3+} results in a lack of an absorption band near 0.9 μm, and the low Fe^{2+} abundance likely accounts for the lack of a prominent Fe^{3+}–Fe^{2+} charge-transfer band near 0.7 μm and expected Fe^{2+} crystal-field transition bands near 0.9 and 1.1 μm.

The presence of OH leads to absorption bands at 1.41 and 2.75 μm, while adsorbed or interlayer H_2O results in the absorption bands at 1.46, 1.9, and 3 μm. Our saponite spectrum differs from that of Clark et al. (1990) in having absorption bands between 2.1 and 2.2 μm, rather than between 2.3 and 2.4 μm. These weak features are likely due to Al–OH and Mg–OH by analogy with other phyllosilicates such as serpentine and halloysite. Upon exposure to lower atmospheric pressures, all of the absorption bands become progressively weaker, with H_2O bands showing greater decrease in intensity than the OH bands. However, once again the various diagnostic absorption bands do not show significant change in positions, given the spectral resolution and signal-to-noise limitations of the data.

3.3. T–O–T + C + T–O–T phyllosilicates—Glauconite

T–O–T + C + T–O–T phyllosilicates are similar to T–O–T phyllosilicates but contain additional cations between adjacent T–O–T planes, versus H_2O in T–O–T phyllosilicates. Glauconite (GLA103) is the only member of this group included in our study; it has not yet been identified as being present on the surface of Mars. The ideal formula of glauconite is $(K,Na)(Fe^{3+},Al,Mg)_2(Si,Al)_4O_{10}(OH)_2$. Our sample contains both Fe^{3+} and Fe^{2+} (Table 2), giving rise to absorption bands near 0.75 μm (Fe^{3+}–Fe^{2+} charge transfer), 0.9 μm (Fe^{3+} and/or Fe^{2+} transitions), and 1.1 μm (Fe^{2+} transitions) (Fig. 2i). The low overall reflectance likely accounts for the lack of a well-resolved OH absorption band near 1.4 μm. The glauconite spectrum is broadly similar to that of the other Fe-rich phyllosilicates, such as berthierine and cronstedtite, in exhibiting a broad region of Fe-related absorption shortward of ~1.8 μm. Adsorbed and/or interlayer H_2O likely accounts for the 1.9 μm absorption band and the broad 3 μm feature, while OH accounts for the absorption band at 2.8 μm. The absorption band at 2.30 μm is attributable to Mg–OH. The identity of the band at 2.36 μm is unknown, but likely due to some metal–OH combination. Upon exposure to lower pressures and UV irradiation, the OH, Fe- and metal–OH related absorption bands are very stable, while the H_2O features at 1.9 and 3 μm decrease in intensity, again due to the liberation of adsorbed and/or interlayer H_2O.

3.4. T–O–T + O + T–O–T phyllosilicates—Clinochlore, chamosite

This phyllosilicate group contains an octahedrally coordinated cation-bearing layer (O) between adjacent T–O–T planes. Clinochlore (chlorite) and chamosite are the two trioctahedral members of this structural group that were included in this study. Both have been tentatively identified on Mars (Poulet et al., 2005; Mustard et al., 2007).

3.4.1. Clinochlore (T–O–T + O + T–O–T trioctahedral)

Clinochlore has an ideal formula $(Mg,Fe^{2+})_5Al(Si_3Al)O_{10}(OH)_8$. Our sample (CLI101) contains both Fe^{3+} and Fe^{2+} (Table 2). This gives rise to the expected Fe^{3+}–Fe^{2+} charge-transfer band (0.7 μm), and Fe^{2+} transition bands near 0.9 and 1.1 μm, with a possible additional contribution from Fe^{3+} to the 0.9 μm band (White and Keester, 1966). It also exhibits a series of sharp absorption bands at 1.39 μm (an OH overtone), and between 2.24 and 2.39 μm. Most or all are attributable to AlOH combinations (King and Clark, 1989).

At longer wavelengths, the initial spectrum exhibits OH absorption bands near 2.717, 2.735, 2.750, 2.800, 2.810, and 2.927 μm (Fig. 2j). These are assigned to OH in the two different O layers, those bonded to the T layer, and those located between adjacent T–O–T sheets (Prieto et al., 1991; Shirozu, 1980). Exposure of the sample to low pressures and UV irradiation results in a gradual loss of fine structure in this wavelength region, with the sharpness of the bands decreasing; i.e., interband peaks gradually disappear. A corresponding loss of fine structure is also seen in the 1.4 μm region. This suggests that low pressures result in a decrease in the degree of crystallinity of clinochlore.

3.4.2. Chamosite (T–O–T + O + T–O–T trioctahedral)

The ideal formula of chamosite is $(Fe^{2+},Mg,Fe^{3+})_5Al(Si_3Al)O_{10}(OH,O)_8$. It differs from clinochlore primarily in containing Fe^{3+} as an integral part of its formula. Our sample (CHM102) is much more Fe-rich than the clinochlore (Table 2). This results in lower overall reflectance and more intense

Fe-related absorption bands (Fig. 2k), which are consequently better resolved than in the clinochlore spectrum. Nevertheless, the expected Fe absorption bands can be identified near 0.7, 0.9, and 1.1 μm. The possible metal–OH absorption bands in the 2.1–2.4 μm region are broad and generally weak, again likely due to the low overall reflectance of the sample. The expected 1.4 μm OH overtone is barely resolvable and the OH-stretching fundamental near 2.75 μm shows no structure. The spectral changes accompanying exposure to low atmospheric pressures and UV irradiation are minor. There are no significant or systematic changes in band positions or intensities, suggesting that chamosite is quite stable under Mars surface conditions.

3.5. Phyllosilicates—Hisingerite

Hisingerite is an incompletely characterized phyllosilicate with structural similarities to the allophone group of micaceous phyllosilicates (Farmer, 1992; Eggleton and Tilley, 1998). Its ideal formula is $Fe_2^{3+}Si_2O_5(OH)_4{\cdot}2H_2O$ and it is an initial weathering product of basalt, consequently its inclusion in this study. Our sample (HIS001) contains all of its Fe as Fe^{3+} and is largely amorphous by XRD (Table 2). The abundance of Fe^{3+} and lack of Fe^{2+} is reflected in the lack of a prominent Fe^{3+}–Fe^{2+} charge-transfer band near 0.7 μm or a prominent Fe^{2+} transition band near 1.1 μm (Fig. 2l). The Fe^{3+} transition band near 0.9 μm is similarly weak, perhaps indicative of the poorly crystalline nature of the sample that prevents the development of OH-bridged Fe^{3+} complexes. OH and H_2O absorption bands near 1.4 and 1.9 μm are weak, as are probable metal–OH combination bands in the 2.1–2.4 μm region. Upon exposure to low pressures and UV irradiation, all the OH and H_2O bands become progressively weaker. The Fe^{3+} band and metal–OH bands are largely unaffected by the changes in environmental conditions, suggesting that the amorphous component is likely accounting for most of the loss of OH and H_2O.

3.6. Palagonitic soil

Terrestrial palagonitic soil is often used as a spectral analog of fine-grained martian dust (Allen et al., 1998). We included a palagonitic soil that has previously been used as a martian spectral analog (Morris et al., 2001) in our experimental run (Table 2). This sample (PAL101) shows minor amounts of plagioclase feldspar, pyroxene, and magnetite by XRD (Morris et al., 2001). Its spectrum is characterized by a sharp rise in reflectance up to ~0.75 μm, and a flatter spectrum toward longer wavelengths, with broad, shallow OH and H_2O absorption bands in the 1.4 and 1.9 μm regions, and a weak metal–OH absorption near 2.1 μm (Fig. 2m). The longer wavelength interval similarly lacks diagnostic absorption features. XRD analysis of the <45 μm dry-sieved fraction used for our study was unable to confidently identify any minerals except for the possible presence of a small amount of albite.

Upon exposure to low atmospheric pressures, the 1.9 μm band became nearly indiscernible, consistent with the results of Bishop and Pieters (1995). The 1.4 and 2.1 μm bands showed no systematic change in intensity, while the 3 μm region showed a decrease in intensity due to the loss of H_2O, but remains the dominant feature (Bishop and Pieters, 1995). A more dramatic change occurred when the sample was subject to pressures of 2.6 Pa: the region below 1.4 μm became more red-sloped, consistent with a decrease in crystallinity of the sample and resulting in a greater range of Fe–O bond lengths. The numerous narrow OH stretching fundamentals in the 2.7–2.9 μm region do not show any compelling evidence for change in position or intensity over the course of the 2.6 Pa exposure. Some of the spectral change is likely due to a change in the surface texture of the sample, perhaps arising from self compaction when the pressure was reduced to a few Pa. The lack of diagnostic absorption features in this material hampers further speculation on possible mechanisms of change.

3.7. Hydroxides—Goethite, diaspore

Hydroxides are important minerals from the perspective of Mars because their presence allows us to constrain the geological and climatic evolution of the planet. Goethite (FeOOH) has been suggested as a probable precursor to the extensive deposits of hematite found in a few places on Mars (Christensen et al., 2001), while diaspore (AlOOH) has been tentatively detected at a few locations on Mars (Bell et al., 2000). The metal–OOH bonding of these minerals is similar to that of the octahedral layers in phyllosilicates.

3.7.1. Goethite

Goethite spectra are characterized by intense Fe^{3+} spin-forbidden, OH-bridged, magnetically-coupled absorption bands near 0.5, 0.65, and 0.9 μm (Mao and Bell, 1974; Sherman et al., 1982; Morris et al., 1985) (Fig. 3a). Our goethite sample (OOH003) contains small amounts of hematite and an unidentified aluminosilicate, likely a phyllosilicate (Table 2). This latter material likely accounts for the weak absorption features near 2.1 μm. The 2.42 μm band is attributable to a goethite Fe–OH combination band (Cloutis and Bell, 2000). The OH-stretching fundamental accounts for the broad absorption feature near 3.2 μm.

Upon exposure to lower atmospheric pressures and UV irradiation, we see no systematic changes in band positions or intensities, although the 2.9 Pa exposure did seem to result in a small increase in the degree of redness of the spectral slope shortward of 1.4 μm. We are uncertain as to the cause of this, but it may be related to a change in the height of the surface of the sample or its surface texture. The inclusion of UV irradiation did not have a measurable effect on the spectral properties of the sample, consistent with previous results concerning the stability of goethite to UV irradiation (Yen et al., 1999).

3.7.2. Diaspore

Diaspore was tentatively identified on Mars on the basis of diagnostic absorption bands near 3.33 and 3.42 μm (Bell et al., 2000). Its identification on Mars would provide compelling evidence for intense and prolonged water circulation. Our diaspore spectrum (OOH012; Table 2) exhibits absorption bands near 1.8 μm, likely attributable to a combination of OH stretching

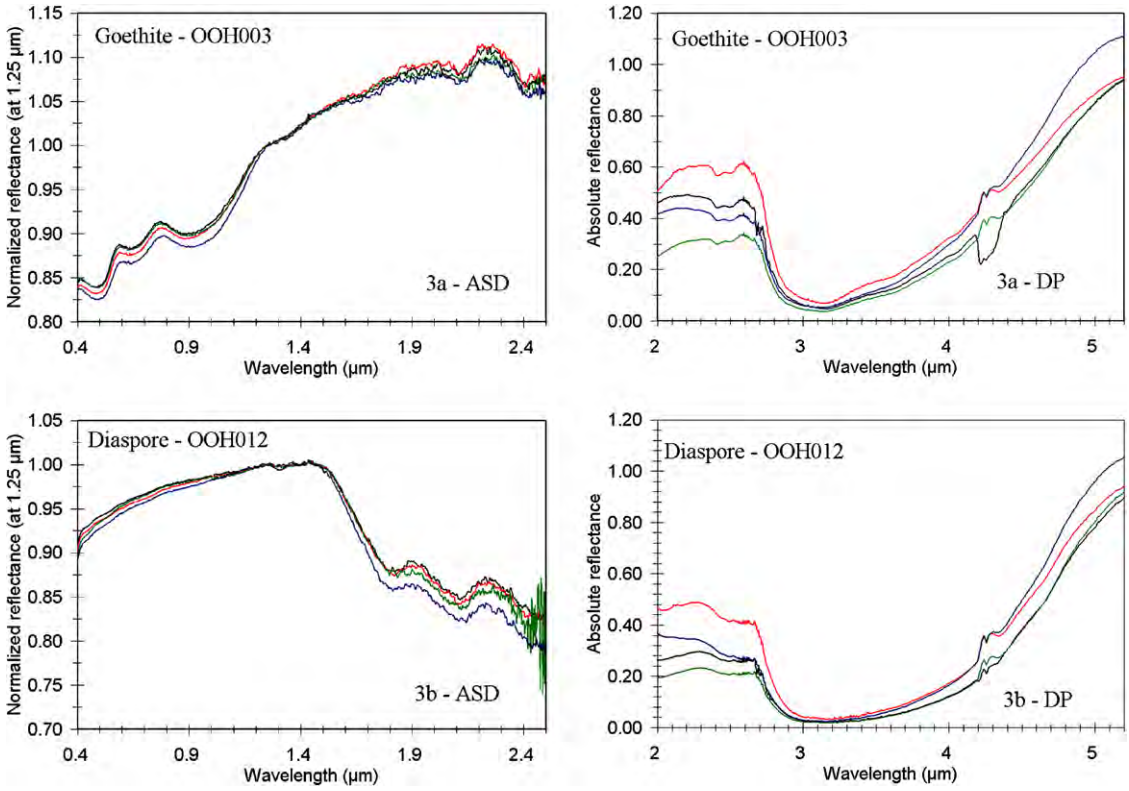

Fig. 3. Same as for Fig. 2 but for hydroxides. (a) Goethite (OOH003); (b) diaspore (OOH012).

and rotation (Cloutis and Bell, 2000), and an additional band near 2.12 µm, attributable to an Al–OH combination (Fig. 3b). The diagnostic absorption bands near 3.33 and 3.42 µm are not well resolved because they lie in a region of low reflectance. Upon exposure to Mars surface conditions, there is a small increase in band intensities in the 1.8 and 2.1 µm regions, but we attribute this to changes in sample height and surface texture, as the same trend is not seen in FTIR spectra. Collectively, these results suggest that diaspore, if present on Mars, is likely stable to dehydration and its diagnostic absorption bands would persist.

3.8. Carbonates—Calcite, magnesite, hydromagnesite

Our experimental run included three different carbonates (calcite, magnesite, and hydromagnesite) as well as two different grain sizes of calcite (<45 and 90–180 µm). The grain size study was designed to investigate whether particle size has a measurable effect on calcite decomposition (Mukhin et al., 1996). Carbonates have been tentatively identified on Mars by a few investigators (Blaney and McCord, 1989; Pollack et al., 1990; Calvin et al., 1994; Lellouch et al., 2000; Bandfield et al., 2003; Hamilton et al., 2005), with magnesite (Blaney and McCord, 1989; Bandfield et al., 2003) and hydromagnesite (Calvin et al., 1994) suggested as candidate species.

3.8.1. Calcite

Calcite (CRB118) was used in our experimental runs because of experimental evidence that it is unstable under current Mars surface conditions due to ultraviolet decomposition (Mukhin et al., 1996). Calcite is characterized by C–O related stretching overtones and fundamentals near 2.10, 2.33, 2.53, 3.34, 3.58, 3.83 and 3.98 µm (Figs. 4a and 4b). While a decrease in overall reflectance was noted over the course of the run, no systematic reductions in intensities of any of these bands was noted. The addition of UV irradiation did not accelerate the rate of overall reflectance decline, which we believe is likely due to self-compaction. Mukhin et al. (1996) found that decomposition rate declined over time and corresponded to alteration of several monolayers over the course of a 4 h experiment. Sample irradiation in their study was provided by a 250 W Hg lamp. What is not known is the flux per unit area, so direct comparison with our results is not possible. Our results suggest that neither UV irradiation nor pressures well below current Mars surface pressures result in a measurable change in spectral properties over the course of ~1 month. Calcite is a largely transparent mineral and it is possible that some photodecomposition took place, but the depth of decomposition may not have been sufficient to affect the reflectance spectra. The decomposition product, CaO, does not have absorption bands in the wavelength region covered by our experiment and its effect would be limited to a change in overall reflectance. Thus we conclude that while photodecomposition of calcite probably occurs, the rate of decomposition is sufficiently low that longer-duration experiments are required to detect it spectrally.

3.8.2. Magnesite

Magnesite has been suggested to explain weak absorption bands in Mars surface and dust spectra (Pollack et al., 1990). The magnesite sample used in our study (CRB114) was con-

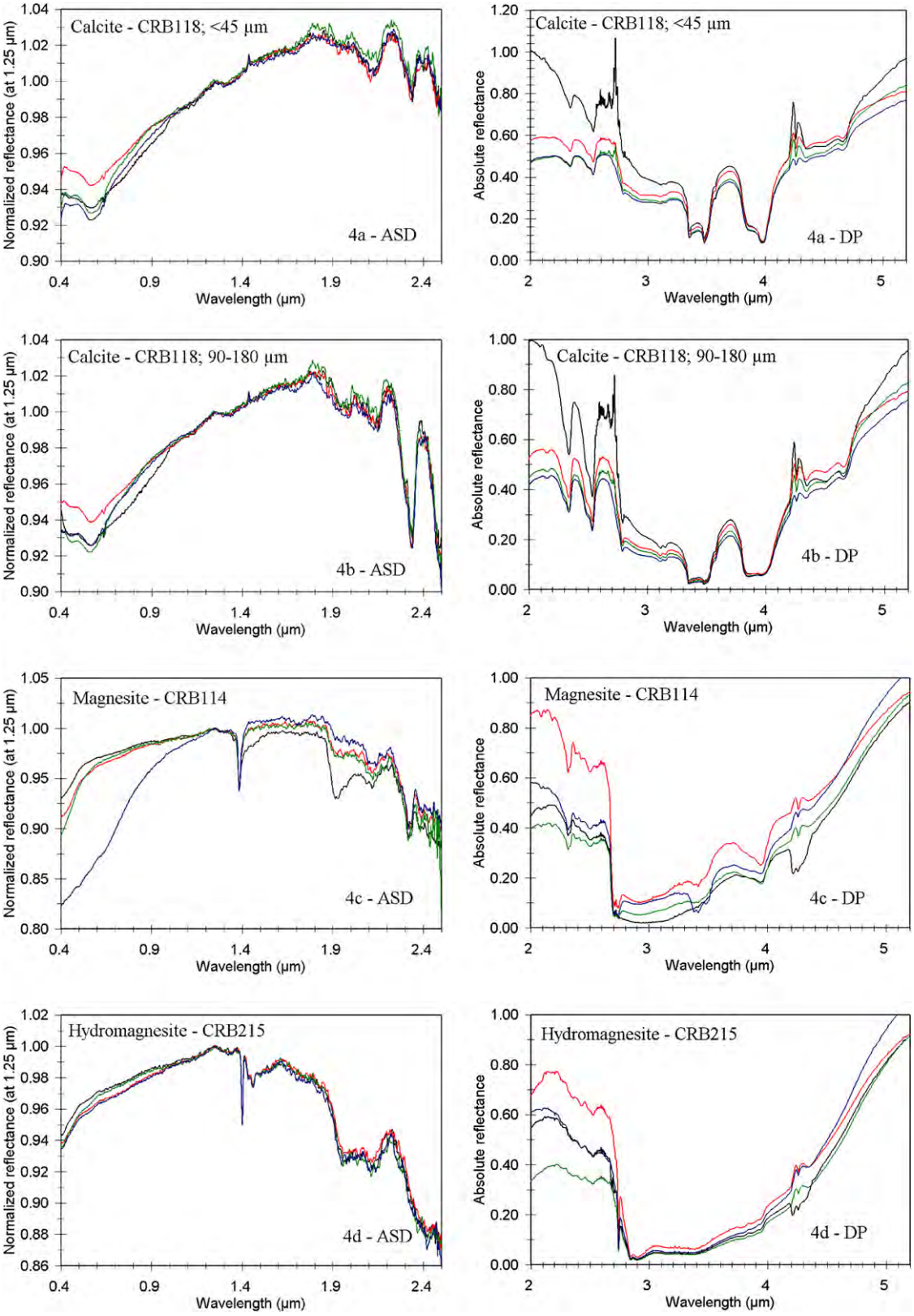

Fig. 4. Same as for Fig. 2 but for carbonates. (a) Calcite, <45 µm (CRB118); (b) calcite, 90–180 µm (CRB118); (c) magnesite (CRB114); (d) hydromagnesite (CRB215).

taminated with a small amount of huntite, another Mg–Ca carbonate and some other unidentified phase to account for the Si detected by XRF (Table 2). Pure magnesite has absorption bands near 2.32, 2.50, 3.28, 3.44, and between 3.80 and 3.95 µm (Fig. 4c). Interpretation of the magnesite spectra is hampered by these accessory phases and the fact that some of magnesite

bands overlap those due to organics (3.3–3.5 μm region). However, it seems that the main carbonate bands at 2.32, 2.5 and 3.80–3.95 μm were not affected by the experimental conditions.

3.8.3. Hydromagnesite

Hydromagnesite is an OH- and H_2O-bearing Mg-carbonate, with an ideal formula $Mg_5(CO_3)_4(OH)_2{\cdot}4(H_2O)$. It has been suggested as a possible explanation for some absorption bands in Mars spectra (Calvin et al., 1994). XRD analysis indicated that the sample used in this study (CRB215) was predominantly hydromagnesite with a small amount of magnesite (Table 2). Its reflectance spectrum exhibits absorption bands at 1.40, 1.43, 1.47 (OH stretching overtones), 1.95 μm (H_2O combination band) and 2.73, 2.84 and 2.90 μm (OH-stretching fundamentals) (Fig. 4d). C–O stretching overtones account for the bands at 2.11 and 2.53 μm. The longer wavelength C–O overtones in the 3.3-4.0 μm region are weak because they are superimposed on the broad H_2O absorption band in this region (Calvin et al., 1994); the most resolvable occur near 3.76, 3.86, and 3.94 μm. Exposure of this sample to lower pressures and UV irradiation had no measurable impact on band position or intensities, suggesting that this mineral is stable under current Mars surface conditions.

3.9. Sulfates

Given the detection of a number of sulfate species on Mars, this study included many sulfate minerals, with an emphasis on those tentatively identified as being consistent with various remote-sensing observations: jarosite (Klingelhöfer et al., 2004), gypsum (Gendrin et al., 2005), polyhydrated sulfate (represented by hexahydrite in this study) (Gendrin et al., 2005), kieserite (Gendrin et al., 2005), copiapite/ferricopiapite (Lane et al., 2007; Johnson et al., 2007), fibroferrite (Lane et al., 2007; Johnson et al., 2007), paracoquimbite (Lane et al., 2007), rhomboclase (Lane et al., 2007; Johnson et al., 2007), szomolnokite (Bishop et al., 2007), paracoquimbite (Johnson et al., 2007), as well as, as yet undetected species, alunite and anhydrite. The sulfates have been subdivided on the basis of hydration type: OH-bearing species (jarosite, alunite), H_2O-bearing species (gypsum, hexahydrite, kieserite, paracoquimbite, rhomboclase, szomolnokite), and OH- and H_2O-bearing species (copiapite, fibroferrite). Additional subdivisions are possible. The H_2O-bearing sulfates include species whose structures consist of isolated SO_4 tetrahedra (hexahydrite), finite clusters of SO_4 polyhedra (paracoquimbite), infinite SO_4 sheets (gypsum, rhomboclase), and an infinite SO_4 framework (kieserite, szomolnokite).

3.9.1. K-jarosite (OH-bearing)

Jarosite has been identified on Mars on the basis of Mössbauer spectra acquired by the Opportunity rover (Klingelhöfer et al., 2004). The 0.4–2.6 μm spectrum of K-rich jarosite (SPT116; Table 2) is characterized by absorption bands at 0.43 and ∼0.9 μm due to Fe^{3+} transitions, 1.465 and 1.51 μm due to OH overtones, 1.84 and 2.27 μm due to OH combinations, and a series of weaker bands in the 2.0–2.6 μm region due to various OH combinations or S–O overtones (Cloutis et al., 2006) (Fig. 5a). At longer wavelengths, K-jarosite exhibits OH-stretching fundamentals at 2.79, 2.94, and ∼3.05 μm. Weak S–O stretching overtones are present near 3.98 and 4.59 μm. The spectra exhibit a high degree of stability over the course of the experiment. The only discernible change is a shift in the position of the 0.9 μm band by ∼10 nm, but this shift is not systematic, and the starting and ending spectra differ by only 2 nm. The other absorption bands show no measurable or significant changes in positions or intensity. These results suggest that K-jarosite is stable at current Mars surface conditions, consistent with thermodynamic calculations (Navrotsky et al., 2005).

3.9.2. Alunite (OH-bearing)

Alunite (SPT129) is the Fe-free Al-bearing analogue of jarosite, but there is limited solid solution between the end members (Brophy et al., 1962; Stoffregen et al., 2000). Alunite spectra are characterized by at least three OH-overtone bands between 1.4 and 1.5 μm, 1.76 and 2.15 μm bands due to OH combinations, and a series of weaker bands from 2.0–2.6 μm due to OH combinations or S–O overtones (Cloutis et al., 2006) (Fig. 5b). It also has a series of narrowly-spaced OH-stretching bands in the 2.7–3.0 μm region. Longer-wavelength S–O overtone bands are weak or absent in our spectra, and some are overlapped by atmospheric CO_2 bands in the 4.2–4.4 μm region.

Upon exposure to Mars surface conditions, the numerous absorption bands are essentially unaffected by the experimental conditions (with the exception of a reduction in two OH absorption bands at 2.68 and 2.70 μm that are not inherent to alunite). This suggests that if alunite were present at the Mars surface its numerous diagnostic absorption bands would allow its detection, and it seems to be very stable.

3.9.3. Hexahydrite (H_2O-bearing)

Hexahydrite (SPT143; Table 2) was included to represent the polyhydrated sulfates postulated to exist on Mars (Gendrin et al., 2005). Identification of a polyhydrated sulfate was based on absorption bands at 1.4 and 1.9 μm, and a 2.4 μm SO stretch in a hydrated environment. These features have asymmetric shapes and plateau-like right wings. Hexahydrite was not identified as a unique match to the OMEGA spectra. The hexahydrite spectra from the experimental run are shown in Figs. 5c and 5d. The hexahydrite is characterized by asymmetric absorption bands centered near 1.42 and 1.92 μm, an S–O stretching overtone band near 2.4 μm, a probable H_2O combination band at 2.5 μm, and a broad and intense H_2O fundamental absorption in the 3 μm region.

Upon exposure to the lower pressure conditions, the H_2O features near 1.42 and 1.92 μm become progressively weaker, resulting in a more “plateau-like” right wing, and hence a better match to this property of the Omega spectra. The two runs show different behavior. In run 1, the atmospheric and 660 Pa spectra are nearly identical, and the addition of UV irradiation seems required to promote reduction in H_2O-related absorption bands. In run 3, no significant changes in band intensities occur until the pressure is reduced to a few Pa. The 2.5 μm feature shows a decrease in intensity as measured relative to the 2.4 μm S–O

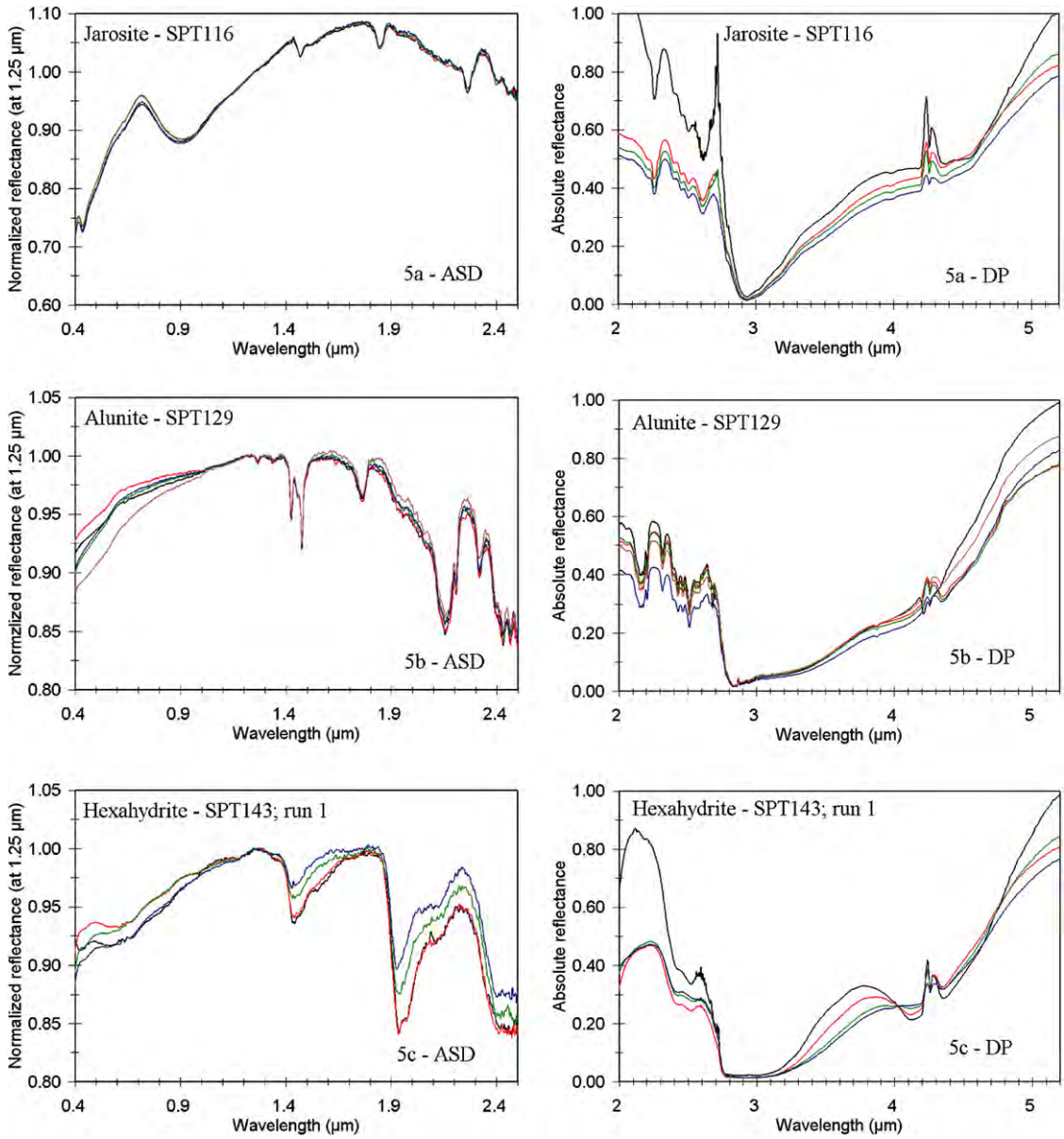

Fig. 5. Same as for Fig. 2 but for sulfates. (a) Jarosite (SPT116); (b) alunite (SPT129); (c) hexahydrite (SPT143, run 1); (d) hexahydrite (SPT143, run 3); (e) kieserite (SPT141); (f) anhydrite + gypsum (SPT128); (g) gypsum (SPT127, run 3); (h) gypsum (SPT127, run 1); (i) rhomboclase (SPT139); (j) szomolnokite (SPT144); (k) paracoquimbite (SPT137); (l) copiapite (SPT117); (m) fibroferrite (SPT121).

band, suggesting that its assignment to H_2O is correct. Within the limits of the data, it does not seem that the positions of the 1.42 and 1.92 µm features change, regardless of the lower ultimate pressure attained (Table 1). The overall spectral changes mimic those seen in heating experiments of polyhydrated Mg-sulfates (Bonello et al., 2005), and more closely resembles the spectra of more H_2O-poor Mg-sulfates (Dalton, 2003).

3.9.4. "Kieserite" (H_2O-bearing)

Kieserite was identified in Omega spectra of Mars on the basis of absorption features at 1.6, 2.1, and 2.4 µm (Gendrin et al., 2005). The 1.6 and 2.1 µm features correspond to the more traditional 1.4 and 1.9 OH/H_2O features, but shifted to longer wavelength in monohydrated sulfates. Kieserite is a somewhat unstable mineral even under terrestrial conditions. We have found that it can show a pronounced color change and some clumping in the course of hand grinding to produce a powder. Thus, spectral data for kieserite must be approached with caution. We found that the kieserite sample prepared for our experimental run was spectrally different from a sample prepared earlier for analysis of sulfate reflectance spectra (Cloutis et al., 2006), and our original sample split was confirmed as kieserite both spectrally and by XRD. Spectra of presumed kieserite measured by different investigators can also show significant differences in shape and band positions (e.g., Dalton, 2003; Bonello et al., 2005; Gendrin et al., 2005; Cloutis et al., 2006).

Our initial "kieserite" sample (SPT141; Table 2) seems to be composed largely of some sort of polyhydrated Mg-sulfate. Given that our presumed kieserite does not match the expected spectral behavior of this mineral, our analysis is tentative. The

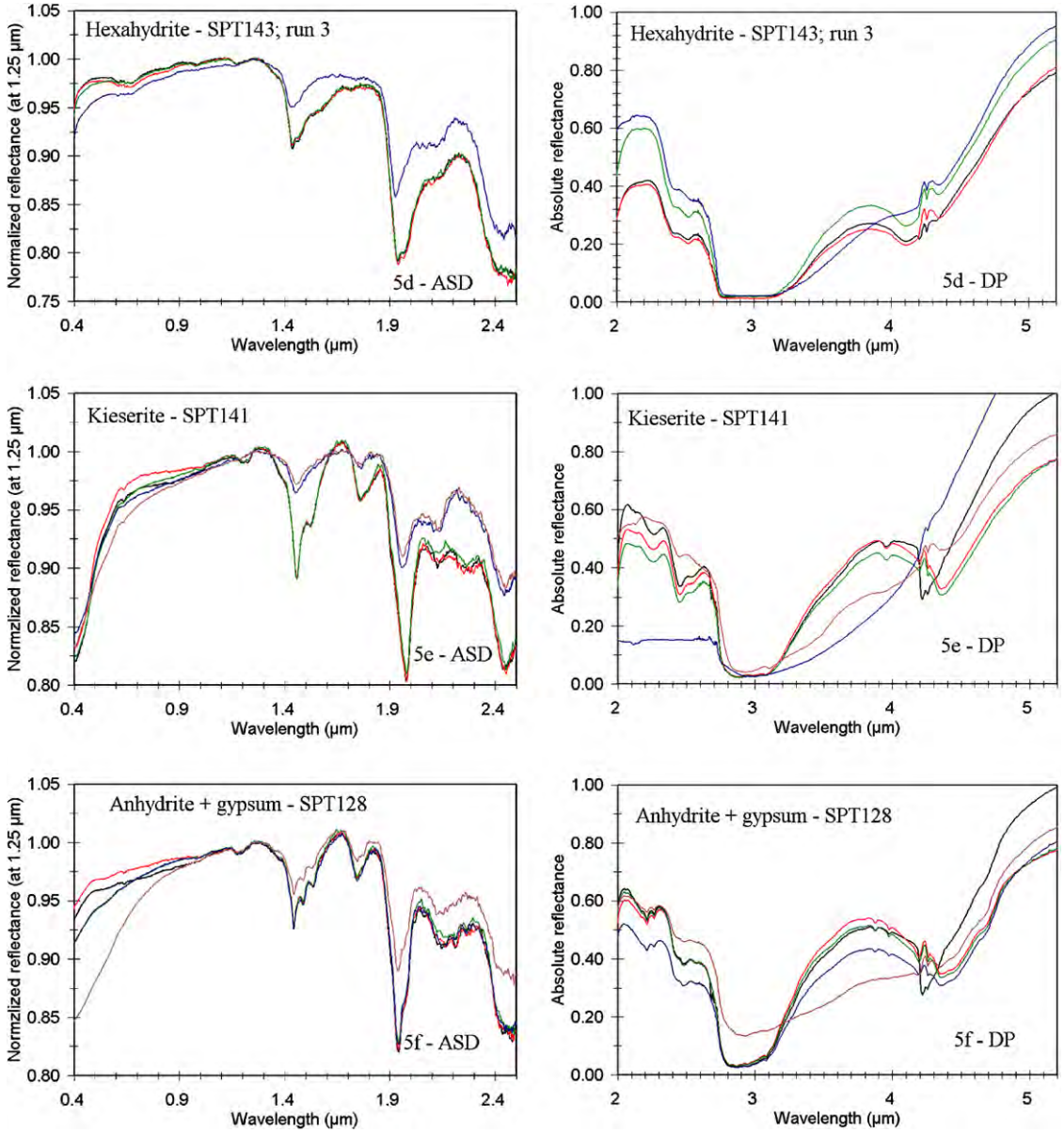

Fig. 5. (*continued*)

spectrum (Fig. 5e) is characterized by two sets of bands in the 1.4 µm region (near 1.47 and 1.52 µm), an OH combination band at 1.76 µm (similar to alunite), H_2O bands at 1.98 and 2.13 µm, a band at 2.26 µm, a presumed S–O stretching overtone at 2.44 µm, and a broad H_2O-related feature in the 3 µm region.

Upon exposure to current Mars surface pressures, there is little change in spectral properties for the 660 Pa and 660 Pa + UV conditions. However, when the pressure was reduced to 1.3 Pa, there is a major change: the 1.4, 1.76, 1.9, and 3 µm region OH and H_2O features become significantly weaker. The spectrum does not, however, become more "kieserite-like," as these absorption bands do not shift to longer wavelengths. The S–O feature near 2.44 µm is unaffected and does not change in position. These results are consistent with other experimental approaches that suggest that dehydration of polyhydrated Mg-sulfates does not normally lead to the formation of kieserite (Vaniman et al., 2004, 2005, 2006; Bish and Scanlan, 2006; Chipera et al., 2005, 2006; Wang et al., 2006a; Freeman et al., 2007b).

3.9.5. *Gypsum (H_2O-bearing)*

Gypsum was identified in Mars Omega spectra on the basis of a series of five absorption bands at 1.4, 1.75, 1.9, 2.2, and 2.4 µm. The 1.4 µm feature consists of three closely spaced bands, while the 2.2 µm feature consists of two bands at 2.21 and 2.27 µm. Three experimental runs were available for gypsum (SPT127: Table 1) (Figs. 5f–5h). Our intention to measure the spectral changes in anhydrite was thwarted by the presence of sufficient gypsum in our anhydrite sample (SPT128; Table 2) to dominate the spectrum. Anhydrite itself is a weak absorber in the 0.4–5 µm region (Cloutis et al., 2006), and gypsum tends to dominate the spectra of many bright materials (Howari et al., 2002).

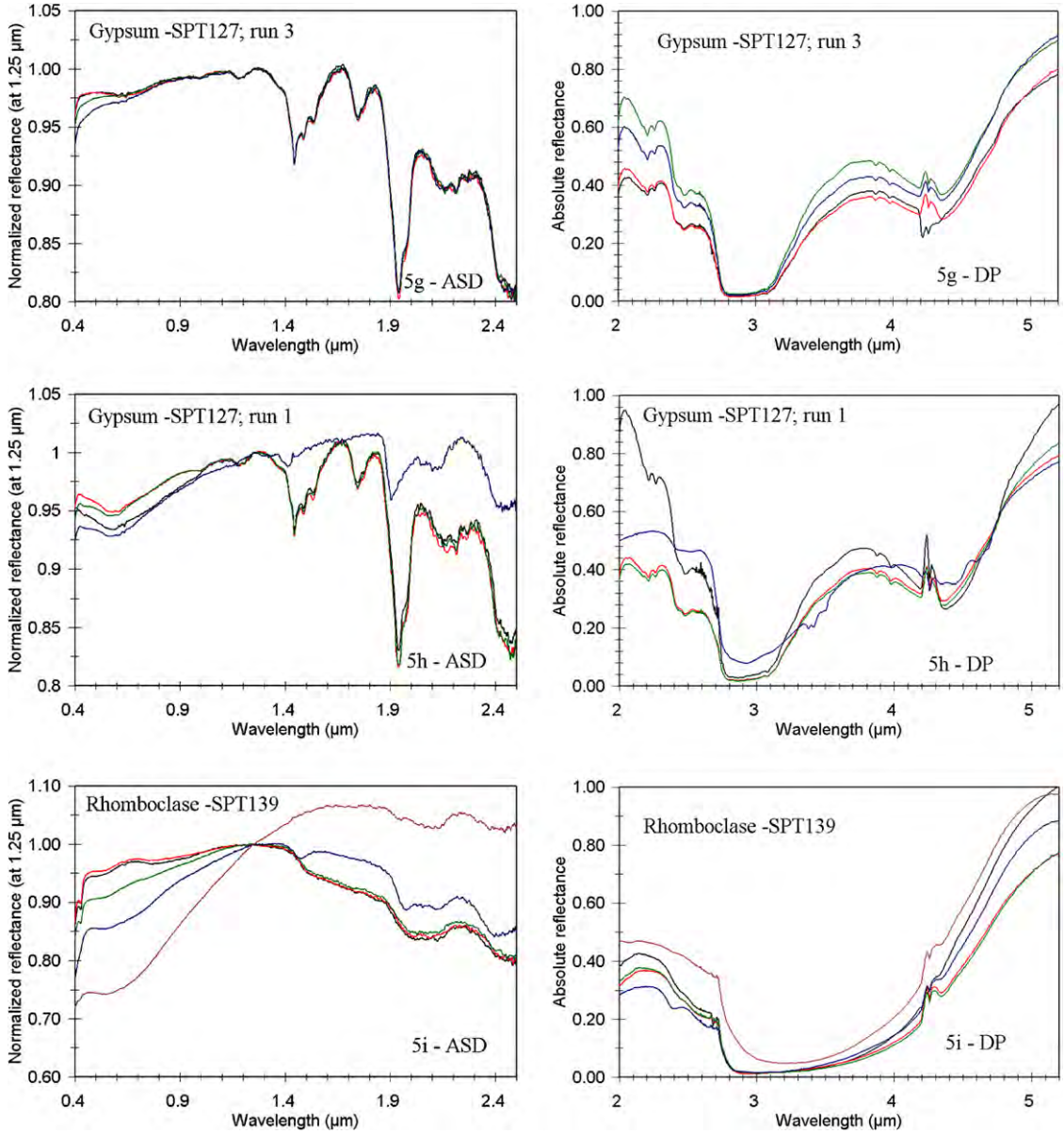

Fig. 5. (*continued*)

The starting spectra of the three samples (the SPT128 sample consists of ~80 wt% anhydrite and ~20 wt% gypsum, while SPT127 is pure gypsum; Table 2) all exhibit a very characteristic triplet of absorption bands of progressively decreasing intensity at 1.44, 1.49, and 1.53 µm (due to O–H stretches), a band at 1.74 µm (due to an OH combination), a double band near 1.94 and 1.97 µm (due to H_2O combinations), a complex feature between 2.1 and 2.2 µm (due to H_2O combinations and/or S–O stretching overtones), an S–O stretching combination at 2.48 µm, and a broad H_2O stretching feature longward of 2.8 µm, all of which are characteristic of gypsum. At longer wavelengths, there are resolvable S–O stretching overtones near 4.46 and 4.67 µm, also attributable to gypsum.

The run 2 data (involving gypsum + anhydrite; Fig. 5f) showed no discernible spectral change for the 660 Pa, 660 Pa plus UV irradiation, or 1.3 Pa portions of the run. However, the addition of UV irradiation to the 1.3 Pa run caused a noticeable reduction in band intensity and a darkening of the sample. We believe that this was due to an unanticipated temperature excursion in our cooling system, and we estimate that the temperature of the sample surface may have reached as high as ~40 °C for 1–2 days. The surface of this sample was visibly darkened at the end of the experimental run. New absorption bands appear in the 4.4–4.7 µm region that are attributable to S–O overtones; such bands are more intense in anhydrite than gypsum (Cloutis et al., 2006). It seems likely that the temperature excursion rather than the UV irradiation led to dehydration of the gypsum. Rapid (a few tens of hours) dehydration of gypsum has been shown for relatively low-temperature (<115 °C) conditions and low relative humidity (47% RH) (Robertson and Bish, 2007). It is also possible that the dehydration observed in the latter part of the experimental run is an acceleration of the gradual dehydration of gypsum that occurs at higher pressures (Vaniman and Chipera, 2006).

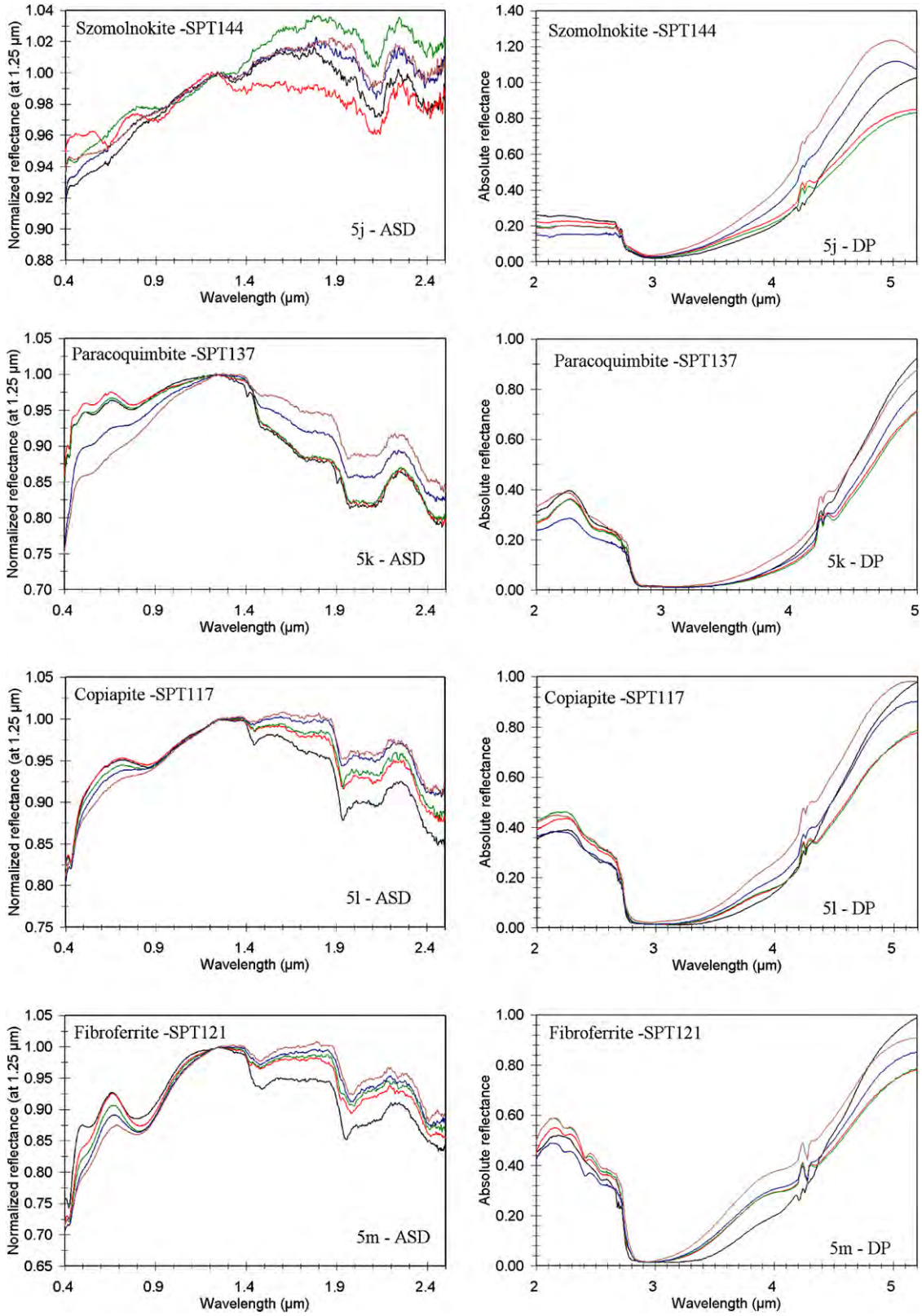

Fig. 5. (*continued*)

For runs 1 and 3, we used pure gypsum (SPT127). The ultimate lower pressure attained during run 3 was 2.6 Pa (Fig. 5g). It is apparent from the data that gypsum showed remarkable stability and no discernible spectral changes were noted. In the case of run 1 (Fig. 5h), we were able to achieve an ultimate lower pressure of 1 Pa and sample temperatures were kept below 25 °C over the duration of the run. As was the case for run 3, there were no discernible spectral changes until the pres-

sure was reduced to 1 Pa. During this portion of the run, the gypsum lost significant H_2O. The spectrum acquired at the end of the run is radically different from that of the starting material. The characteristic absorption-band triplet in the 1.4 μm region is nearly unrecognizable, the 1.74 μm OH combination band is no longer present, the 1.9 μm OH band is reduced in intensity and shifted to shorter wavelength, and the center of the 2.1–2.2 μm feature has also shifted to shorter wavelength. The 2.48 μm S–O overtone is still present but also shifted to shorter wavelength. The 3 μm region OH-stretching fundamental is also reduced in intensity, and the 4–5 μm region of S–O overtones shows new bands.

Pure anhydrite has no strong absorption bands below ∼4 μm (Cloutis et al., 2006). The end-of-run spectrum indicates that the gypsum has undergone significant loss of H_2O but has not totally dehydrated (because a 1.9 μm feature persists; this is consistent with the spectrum of bassanite; Crowley, 1991). This dehydration was accompanied by a structural rearrangement as evidenced by changes in the wavelength positions of the remaining H_2O bands and the appearance of new S–O overtones between 4.4 and 4.7 μm. Anhydrite S–O stretching overtones differ from those of gypsum in this region and the new bands are consistent with anhydrite. Collectively, these results suggest that gypsum is likely stable for extended periods of time under current Mars surface conditions, but will dehydrate rapidly under the influence of modest temperature excursions (Vaniman and Chipera, 2006).

3.9.6. Rhomboclase (H_2O-bearing)

Rhomboclase (ideal formula $[HFe^{3+}(SO_4)_2{\cdot}4H_2O]$) has been suggested as a possible constituent of the Paso Robles soil at Gusev crater on the basis of having a convex-upward inflection at 480 nm in Pancam spectra (Lane et al., 2007). The reflectance spectrum of the initial rhomboclase (SPT139; Table 2) clearly shows this behavior (Fig. 5i). Rhomboclase was part of run 2 which, as mentioned, experienced a temperature excursion during the latter part of the run. Spectrally, it exhibits an Fe^{3+} spin-forbidden band near 0.43 μm, and additional weaker Fe^{3+} bands near 0.53 and 0.79 μm, beyond 1.4 μm, it exhibits gradually decreasing reflectance due to a combination of an H_2O stretching absorption beyond ∼1.45 μm, the OH combination band in the 1.75 μm region, H_2O combination bands in the 2 μm region, and H_2O combination bands and/or S–O stretching overtones beyond 2.4 μm and the short wavelength wing of the intense H_2O fundamental in the 3 μm region. The lack of OH results in a lack of sharp absorption bands in the 1.4 and 2.8 μm regions.

Exposure to martian surface conditions seems to have little effect on the diagnostic absorption bands, beyond a modest decline in visible reflectance. When pressures were reduced to 1.3 Pa, significant dehydration began, resulting in a loss of the 1.75 μm region OH band, the appearance of some structure in the 1.9–2.2 μm region (perhaps due to a loss of an H_2O absorption band near 2.05 μm), and the appearance of a resolvable S–O overtone band at 2.40 μm. The absorption bands due to OH-bridged Fe^{3+} also became less distinct, suggesting loss of Fe^{3+}–Fe^{3+} bridging OH. The inadvertent sample heating that occurred during the 1.3 Pa + UV irradiation part of the run resulted in further spectral changes, largely a loss of Fe^{3+} and H_2O absorption bands. Collectively, the results suggest that rhomboclase is stable under current Mars surface conditions but that modest higher-temperature excursions can result in the loss of some H_2O and hence modifications of the characteristic Fe^{3+} bands and overall spectral shape.

3.9.7. Szomolnokite (H_2O-bearing)

Szomolnokite (ideal formula $Fe^{2+}(SO_4)(H_2O)$) should exhibit an Fe^{2+}-related absorption feature in the 1 μm region and have H_2O absorption bands similar to kieserite (Bishop et al., 2007). Our szomolnokite spectrum (SPT144) exhibits less intense absorption bands than that of Bishop et al. (2007). Our sample is contaminated with a number of accessory phases (Table 2), but still shows the characteristic features of szomolnokite: an Fe^{2+} absorption band near 0.9 μm, a broad 1.4 μm region H_2O absorption, and an H_2O combination band with a minimum near 2.1 μm (Fig. 5j). The longer-wavelength region is dominated by the H_2O absorption near 3 μm, and S–O stretching fundamentals are not apparent at longer wavelengths. The lower-wavelength spectra are noisy but still suggest that this mineral is largely stable under current Mars surface conditions. The Fe^{2+} absorption band near 0.9 μm persists, and the diagnostic absorption band near 2.1 μm does not change in position.

3.9.8. Paracoquimbite (H_2O-bearing)

Coquimbite has been identified as a possible constituent of the Paso Robles soils at Gusev Crater from analysis of Pancam data on the basis of spectral mixture modeling (Johnson et al., 2007) and specific spectral features: a convex-upward inflection at 480 nm, a reflectance maximum at 670 nm, and a reflectance minimum between ∼750 and 850 nm (Lane et al., 2007). Paracoquimbite (SPT137) is an Fe^{3+}-bearing hydrated sulfate with an ideal formula $Fe_2^{3+}(SO_4)_3{\cdot}9H_2O$. Spectrally, it exhibits Fe^{3+}-related absorption bands near 0.43, 0.47, 0.55 and 0.78 μm (Fig. 5k). Like rhomboclase, it exhibits decreasing reflectance longward of 1.3 μm due to a variety of mostly H_2O-related absorption bands. It has some spectral similarities to kieserite as well, exhibiting a broad H_2O absorption that extends from ∼1.95 to 2.15 μm, and an S–O overtone band near 2.45 μm. There are no well-defined S–O overtone bands in the 4-5 μm region.

Exposure to Mars conditions has no apparent effect on the Fe^{3+} or H_2O absorption bands: the spectrum is essentially unchanged. However, when exposed to the 1.3 Pa pressure environment, H_2O absorption bands become weaker and the fine structure in the Fe^{3+} absorption bands is lost, likely due to disruption or loss of Fe^{3+} bridging H_2O molecules. The 1.3 Pa plus UV irradiation (plus inadvertent heating) leads to accelerated loss of detail in the Fe^{3+} bands and reductions in H_2O band intensities.

3.9.9. Copiapite (OH- and H_2O-bearing)

Copiapite was identified as a possible constituent of Paso Robles soils at Gusev Crater on the basis of a reflectance max-

imum near 670 nm in Pancam spectra (Lane et al., 2007) and from spectral mixture analysis (Johnson et al., 2007). Its ideal formula is $Fe^{2+}Fe_4^{3+}(SO_4)_6\cdot(OH)_2\cdot 20H_2O$ (SPT117, Table 2). Spectrally, it exhibits absorption bands attributable to Fe^{3+}: hydroxo-bridged Fe^{3+} absorption bands near 0.43 and 0.87 μm (Fig. 5l). OH likely accounts for the sharp absorption feature near 1.45 μm, while H_2O likely accounts for the absorption feature between 1.92 and 2.15 μm. The copiapite spectrum of Bishop et al. (2007) does not exhibit the 1.45 μm band, and also shows a narrower 1.92–2.15 μm feature, but the Fe^{3+} features are common to both spectra. At longer wavelength, no distinct OH-stretching fundamentals are seen; they are likely obscured by the broad H_2O band near 3 μm.

Exposure to Mars surface conditions causes both the 1.45 μm OH and 1.92–2.15 μm H_2O absorption features to decrease in intensity. Exposure to 1.3 Pa pressures causes a reduction in the intensity of the 0.43 μm Fe^{3+} absorption band and flattening out of the spectrum in the area of the 0.87 μm Fe^{3+} absorption band. This is accompanied by further reductions in OH and H_2O band intensity. The major effect of the final UV (+heating) exposure is to cause further reduction in Fe^{3+} band intensities.

3.9.10. Fibroferrite (OH- and H_2O-bearing)

Fibroferrite has an ideal formula $Fe^{3+}(SO_4)(OH)\cdot 5H_2O$ (SPT121; Table 2). It exhibits Fe^{3+}-related absorption bands at 0.43, 0.55 and 0.80 μm, all attributable to hydroxo-bridged Fe^{3+}. It was also suggested as a possible component of Paso Robles soils from comparison to Pancam data (Lane et al., 2007; Johnson et al., 2007). It has many similarities to copiapite but with better-defined Fe^{3+} bands (Fig. 5m). The spectral changes accompanying exposure to Mars surface conditions mimic those of copiapite: decreases in OH and H_2O band intensities and loss of detail in the Fe^{3+} bands, accompanied by a shift in the 0.8 μm band to slightly higher wavelengths. New absorption bands appear near 2.25 and 2.4 μm, and the positions and number of bands in the 1.9–2.1 μm region change, suggesting formation of a new phase. The 1.3 Pa conditions do not result in any new spectral changes but are merely continuations of existing changes.

3.10. Organic-bearing materials—Oil sand, oil shale, gilsonite

Three organic-bearing geological materials (oil sand, oil shale, gilsonite) were included in this study to determine how organic materials are affected by exposure to Mars surface conditions. These three materials contain a wide range of organic molecule types and sizes, but are generally condensed and of low volatility. Thus they are suitable for examining the stability of evolved organics. Organic materials are generally characterized by C–H absorption bands in the 1.7, 2.15, 2.3–2.5, and 3.4–3.5 μm regions due to aliphatic C–H stretching fundamentals and overtones, and near 3.15 μm for aromatic C–H stretches.

3.10.1. Athabasca oil sands

Athabasca oil sands consist largely of quartz sand with very minor amounts of clay minerals and a complex organic component (bitumen) composed of a wide variety of organic molecules, mostly large aromatic molecules, many being heterocyclic with short aliphatic side chains (Bichard, 1987). Our sample (TAR17) contains 80.9 wt% mineral grains >45 μm in size (almost exclusively quartz), 3.5 wt% <45 μm mineral grains (composed largely of quartz with lesser amounts of various phyllosilicates) and 15.6 wt% bitumen. Spectrally it exhibits the expected aliphatic absorption features in the 1.7, 2.15, 2.3–2.5, and 3.3–3.5 μm regions (Fig. 6a). Upon exposure to Mars surface conditions there is no systematic change in the appearance of the organic absorption bands or the relative intensities of the aliphatic versus aromatic absorption bands in the 3.15–3.5 μm region, as would be expected with further condensation of the organic component.

3.10.2. Oil shale

Our sample of oil shale from the Colorado oil shale deposit (OILS10) consists largely of phyllosilicates (84%) and hydrocarbons (14%) with an H/C ratio of ∼1.5 (Hunt, 1979). The hydrocarbon fraction consists of insoluble kerogen (∼85%) and soluble bitumen (∼15%) (Mang, 1988). The kerogen is predominantly cyclic, with 45–60% heterocyclics, 20–25% naphthene hydrocarbons, 10–15% aromatics, and 5–10% normal and isoparaffins (Hunt, 1979). It has some spectral similarities to the Athabasca oil sand, exhibiting all of the expected C–H absorption bands (Fig. 6b). The rise in reflectance longward of 3 μm is steeper than for the Athabasca oil sand, likely due to the lower abundance of aromatic molecules. As was the case with the oil sand, exposure of this sample to Mars surface conditions did not lead to any measurable changes in organic absorption-band intensities or changes in aromatic:aliphatic band intensity ratios.

3.10.3. Gilsonite

Gilsonite is a high-asphaltene organic material that is soluble in aromatic and aliphatic solvents, and is also commonly known as asphaltite. It has a lower H/C ratio than the Colorado oil shale (∼1.35) and is broadly similar to the heaviest fraction of the Athabasca oil sand (Hunt, 1979). Our sample (GIL101) is essentially mineral-free. The complex organic nature and high aromaticity results in low overall reflectance and relatively weak aliphatic absorption bands in the 1.7, 2.15, and 2.3–2.5 μm regions (Fig. 6c), with correspondingly better-resolved aromatic absorption features near 3.15 μm, and fundamental aliphatic C–H absorption bands between 3.35 and 3.5 μm. Exposure of the sample to simulated Mars surface conditions does not cause any systematic changes in organic absorption-band intensities or positions.

4. Discussion

As expected, given the diversity of samples used in the experiments, few general trends are present. Nevertheless, some general and more specific observations can be made.

For the phyllosilicates, structural OH is generally retained, most of the OH overtone bands near 1.4 μm in the phyllosilicate spectra are unchanged, both in terms of intensity and positions.

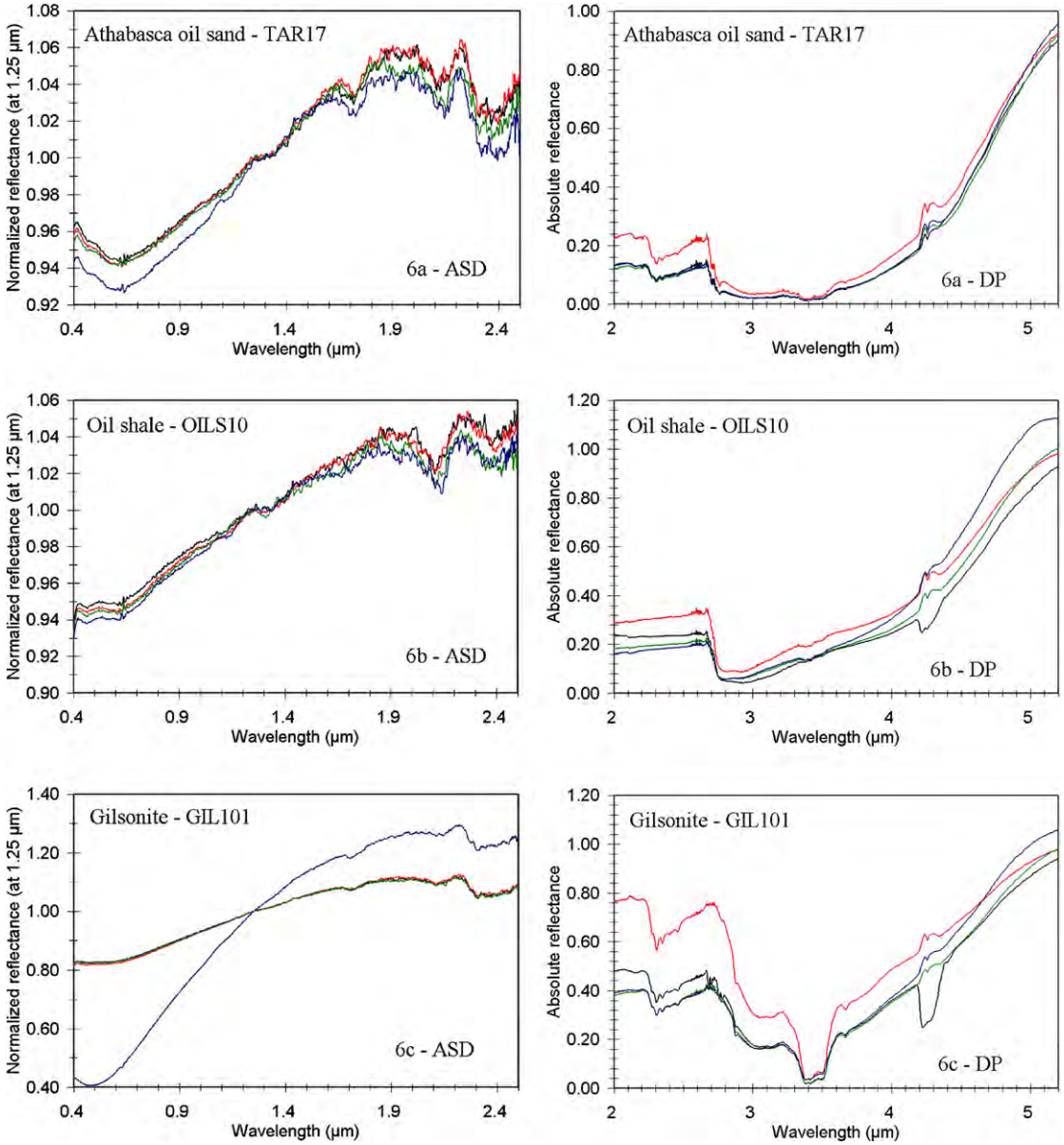

Fig. 6. Same as for Fig. 2 but for hydrocarbon-bearing geological materials. (a) Athabasca oil sand (TAR17); (b) Colorado oil shale; (c) gilsonite.

Similarly, metal–OH combination bands in the 2–2.5 µm region are also insensitive to change in experimental conditions. Phyllosilicate identifications on Mars are largely based on these characteristics (Poulet et al., 2005), and the experimental results suggest that these identifications are robust.

The effect of Mars surface conditions on Fe-bearing phyllosilicates is not as systematic. The nontronite sample showed a change in the appearance of the Fe-related absorption feature in the 1-µm region, possibly due to loss of OH and/or a structural rearrangement. It should be noted that this change only occurred when the pressure was reduced to ~1% of current Mars surface pressure. None of the other Fe-bearing phyllosilicates exhibited a similar spectral change.

Spectral discrimination of most phyllosilicates is straightforward, provided it is based on spectrally stable and diagnostic features. The experimental runs show that the intensity of the 1.9 µm H_2O absorption feature in the smectite spectra is reduced upon exposure to low-pressure conditions (Bishop and Pieters, 1995). However, this feature is not particularly diagnostic of a specific phyllosilicate. Phyllosilicate discrimination is best achieved through determining positions of OH overtones in the 1.4-µm region and metal–OH combination bands in the 2.1–2.5 µm region. Our analysis shows that Fe-poor phyllosilicates can be discriminated using these features, with the exception of closely related species such as beidellite and montmorillonite, which have very similar spectra (Figs. 2e and 2f). Spectral similarities also exist for some of the Fe-rich phyllosilicates, specifically berthierine (Fig. 2c) and chamosite (Fig. 2k). Both exhibit Fe^{2+} and Fe^{3+}-associated absorption bands near 0.7, 0.9, and 1.1 µm, a very weak OH absorption feature near 1.4 µm, and FeOH absorption bands in the 2.1 and 2.35–2.5 µm regions.

Loss of a large proportion of H_2O from the phyllosilicates occurred at Mars surface conditions. However, H_2O loss was

not complete as evidenced by the fact that the 3 μm H_2O-stretching fundamental did not completely disappear. The entire surface of Mars shows evidence of a 3-μm feature of varying intensity (Erard et al., 1991; Jouglet et al., 2007), while areas exhibiting a 1.9-μm feature (which is harder to identify due to atmospheric absorptions and overlapping absorptions from pyroxenes) are few in number and extent (Murchie et al., 2000; Jouglet et al., 2007). A persistent 3-μm feature and greatly reduced 1.9 μm band is consistent with many of the phyllosilicates and H_2O-bearing sulfates exposed to Mars surface conditions in our study.

The palagonitic soil showed similar behavior to the phyllosilicates. Palagonitic soil has been used extensively as a spectral analogue for Mars bright (presumably dust-rich) spectra, although it has been noted that the Mars and palagonitic soil spectra differ in palagonitic soil exhibits a well-resolved 1.9-μm absorption feature that is largely absent in Mars bright-region spectra (Allen et al., 1998; Allen and Morris, 1999). Our experimental runs show that palagonitic soil can show a strong reduction in the intensity of the 1.9-μm feature while retaining its characteristic spectral shape at lower wavelengths when exposed to low atmospheric pressures. Interestingly, heating of palagonitic soil to 160 °C causes changes in overall spectral shape and may or may not be accompanied by a significant reduction in 1.9 μm absorption band intensity (Bruckenthal, 1987; Cloutis and Bell, 2004).

Loss of OH from the various samples is dependent on sample type and structure. For the phyllosilicates, only the T–O–T group and the halloysite showed decreases in the intensity of the 1.4-μm OH band, suggesting that this group is more sensitive to low pressure excursions than other phyllosilicate groups. The other phyllosilicate groups and the metal hydroxides did not exhibit significant and systematic decreases in the intensity of the 1.4-μm region OH band. The sulfate group showed more diverse behavior. The OH-bearing sulfates jarosite and alunite seem insensitive to changes in environmental conditions. The OH- and H_2O-bearing sulfates, copiapite and fibroferrite exhibited decreases in 1.4-μm region band intensities, consistent with loss of OH.

Loss of H_2O from the various samples is sensitive to how the H_2O is bound. For the phyllosilicates, H_2O is generally present as weakly bound interlayer H_2O and hence can readily be removed by lowering atmospheric pressure (Bishop and Pieters, 1995). For other minerals such as hydromagnesite and gypsum, the H_2O is integral to the structure and hence is not lost under Mars surface conditions. Many of the sulfate minerals exhibit intermediate behavior: some H_2O may be lost when the pressure is reduced to that of the martian surface.

The inclusion of UV irradiation in the experiments generally did not seem to change the rate of decomposition or loss of H_2O as expressed in changes in the reflectance spectra. While decomposition due to UV irradiation seems to be a viable process for some minerals (Mukhin et al., 1996; Prieto-Ballesteros et al., 2007), it is likely that the time required for UV-related decomposition to appear in reflectance spectra is longer than the duration of these experiments (Mukhin et al., 1996; Yen et al., 1999). The best evidence for UV-enhanced decomposition is shown by the hexahydrite spectra from run 1. In the 1.9-μm region, the initial and end of 660 Pa spectra are nearly identical, while the 660 Pa + UV spectrum shows a decrease in band depth. However, this effect was not reproduced in run 3. The other minerals did not show spectral evidence for UV-enhanced decomposition. However, as noted, UV irradiation in run 2 was accompanied by an inadvertent higher temperature (~40 °C) excursion, complicating attempts to discern UV irradiation from low atmospheric pressure effects.

Changes in experimental conditions had variable effects on Fe-related absorption bands in phyllosilicates. A number of the Fe-bearing samples were insensitive to any change in experimental conditions (e.g., cronstedtite, berthierine, glauconite). Others, such as nontronite, showed spectral changes consistent with a loss of Fe-bridging OH; i.e., change in appearance of 0.9 μm OH-bridged Fe^{3+} spin-forbidden transition (Sherman and Vergo, 1988) and the width of the OH-stretching fundamentals near 2.7 μm. However, this was not accompanied by a similar change in the intensity, position or width of the Fe–OH absorption band at 2.29 μm. The loss of spectral detail in the 2.7 μm region, where absorption bands are attributable to OH-stretching fundamentals, is likely due to a structural rearrangement of bridging OH.

Spectral changes in the phyllosilicates do not always mean that new phases were formed. In the case of the smectites, reduction in H_2O absorption intensities is not associated with the formation of a new phase, as variable amounts of interlayer H_2O can be accommodated within a specific species. For the smectites and the other phyllosilicates, reductions in the intensity of the 1.4 μm OH absorption features implies formation of a new phase, as OH is an integral part of the structure. However, the nature of these new phases could not be ascertained, as intensity reductions were generally not accompanied by shifts in the positions of the OH and metal–OH absorption bands or the appearance of new absorption bands. The situation was similar for the absorption bands due to Fe in nontronite. While the Fe absorption bands showed evident spectral change, the identity of any new phases that were forming could not be ascertained from the reflectance spectra.

The sulfates showed more dramatic effects. With the exception of jarosite (expected to be stable on Mars; Navrotsky et al., 2005), all the Fe^{3+}-bearing sulfates exhibited a decrease in the intensity of the OH-bridged Fe^{3+} absorption band near 0.43 μm, as well as other spectral changes to the additional Fe^{3+} bands at longer wavelengths (Fig. 7); the decrease in band intensity occurs largely during the low-pressure (few Pa) part of the experimental runs. These samples also visibly darkened over the course of the experiment. The results suggest that Fe^{3+}-bearing sulfates, if present at some depth where they are not exposed to the full effects of the martian surface, could change both spectrally and visually over short time frames. Phase changes are expected for some Fe-bearing sulfates exposed to martian surface conditions (Xu et al., 2007). The results also suggest that the characteristic Fe^{3+} absorption band near 0.43 μm indicates the presence of jarosite rather than some other Fe^{3+} sulfate.

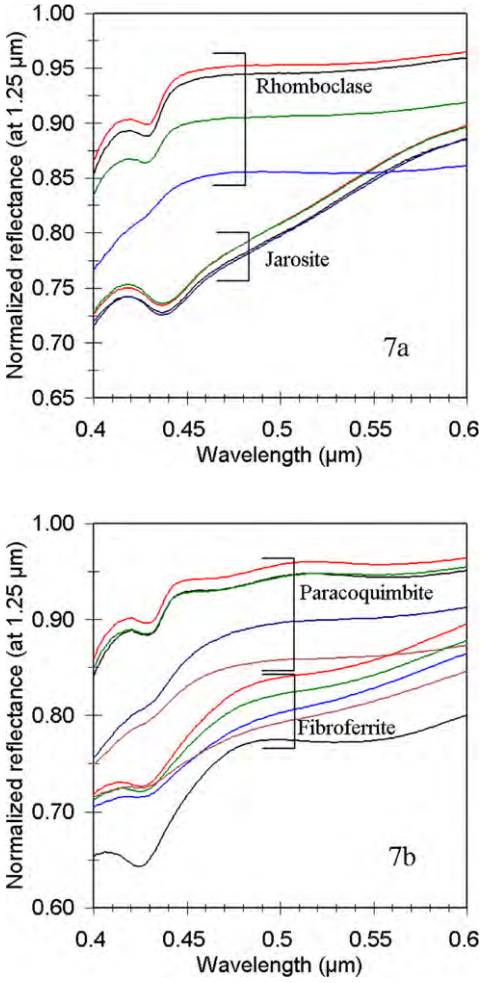

Fig. 7. Details of the spectra in the 0.4–0.6 µm region from the experimental runs for: (a) rhomboclase (SPT139), jarosite (SPT116); (b) paracoquimbite (SPT137), fibroferrite (SPT121). The spectra are color-coded using the same color scheme as in Fig. 2.

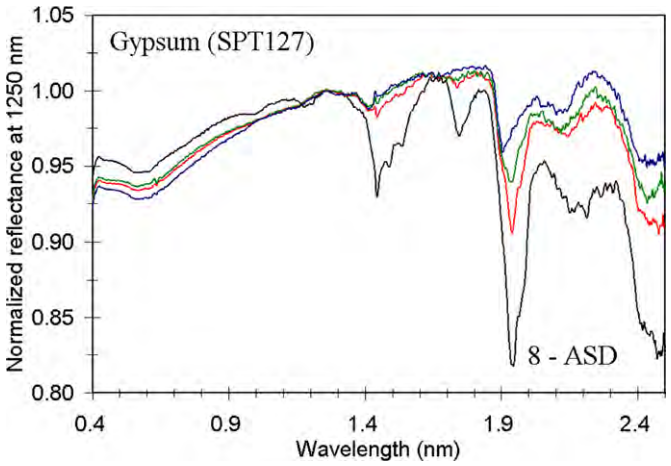

Fig. 8. Reflectance spectra of gypsum acquired during run 1. Spectra are as follows: black, end of 660 Pa + UV irradiation; red, 6 days into 1 Pa exposure; green, 8 days into 1 Pa exposure; blue, 25 days into 1 Pa exposure (end of run).

While many of the sulfates did show spectral changes over the course of the experimental runs, in many cases the identities of presumed new phases could not be confidently assigned, although phase changes would likely occur for some hydrated species (Chipera et al., 2007; Wang et al., 2007; Xu et al., 2007). The fibroferrite spectrum (Fig. 5m) provides a good example. Exposure to martian surface conditions caused changes in the shapes and positions of the absorption features near 1.4 and 1.9 µm. These changes suggest loss of OH and H_2O and structural rearrangement. The closest spectral analogues to altered fibroferrite are copiapite and coquimbite, in terms of an Fe^{3+} absorption band beyond 0.8 µm, a weaker 1.4 µm OH band, and the shape of the 1.9 µm absorption feature (Cloutis et al., 2006). Both species are less hydrated than fibroferrite.

The hexahydrite spectra suggest partial transformation of hexahydrite to starkeyite (the 4-hydrate) based on changes in the shape of the 1.9-µm region H_2O absorption band (Crowley, 1991). Such a transformation, with starkeyite being a major product, is known to proceed rapidly (~1 day) at relatively low temperatures (0–75 °C) and relative humidities (Chipera et al., 2006; Wang et al., 2006a, 2007). There is no spectral evidence for the formation of kieserite from the hexahydrite, as this pathway does not seem to be viable at our experimental conditions (Freeman et al., 2007b). Kieserite can form from hexahydrite at other conditions (Chipera and Vaniman, 2007). Similarly there is no spectral evidence for the formation of an expected amorphous Mg-sulfate phase (Vaniman et al., 2004; Wang et al., 2007). However, reflectance spectroscopy is not well suited to detecting this transformation.

The gypsum spectrum from run 1 shows the clearest evidence for formation of a specific new phase. Fig. 8 shows spectra taken over the course of the low-pressure (1 Pa) exposure. There are three associated Ca-sulfate minerals: gypsum ($CaSO_4 \cdot 2H_2O$), bassanite ($CaSO_4 \cdot 0.5H_2O$), and anhydrite ($CaSO_4$). The major spectral differences between gypsum and bassanite are the absorption feature between 1.4 and 1.55 µm exhibiting three (gypsum) or two (bassanite) resolvable absorption bands and a shift in the position of the main band from ~1.43 (gypsum) to ~1.41 µm (bassanite), the absorption feature between 1.7 and 1.8 µm consisting of two (gypsum) or one (bassanite) resolvable band, and the position of the main band shifting from ~1.73 (gypsum) to ~1.76 µm (bassanite), the absorption feature near 1.93 µm consisting of two (gypsum) or one (bassanite) absorption band, and the main band shifting from ~1.93 (gypsum) to 1.90 µm (bassanite), the appearance of an absorption band near 2.09 µm in bassanite but not in gypsum, and the appearance of an absorption band at 2.20 µm in gypsum but not in bassanite (Crowley, 1991). Fully dehydrated anhydrite is nearly spectrally featureless in the 0.4–2.5 µm region (Cloutis et al., 2006). Comparing the spectra taken at the start, middle and end of the 1 Pa part of the run (Fig. 8), we can see clear evidence of the formation of bassanite over this period, as all of the characteristic spectral features of this mineral appear. Our results suggest that gypsum dehydration can rapidly proceed at ambient temperatures, provided atmospheric pressure is lower. The differences between the transformation at 1 vs 2.6 Pa for gypsum suggest, however, that this transformation is likely kinetically inhibited.

The hydroxide and carbonate minerals do not exhibit spectral changes that are either significant or that imply formation of new phases. For the organic materials as a group, there were no apparent systematic spectral changes. C–H absorption bands did not exhibit significant and systematic change as the experiments proceeded, suggesting that structural or compositional changes, such as aromatization, if active, occurred at a level insufficient to produce measurable spectral change.

The results for nontronite, gypsum and the Fe^{3+}- and H_2O-bearing sulfates, in particular, lead to the question of the full significance of the experimental results. Spectral changes for these minerals were greatest when the pressures were reduced to a few Pa, or roughly two orders of magnitude less than current Mars surface pressure. These low-pressure conditions were included in order to better simulate long periods of time at current Mars surface pressures; they were not meant to imply that Mars may have experienced periods of low atmospheric pressure (a few Pa) in the past and the consequent implications for mineral stability. However, an unknown factor in the assumption is whether short-duration exposures of samples to pressure of a few Pa are reasonable analogues of long-duration exposures to pressures of a few hundred Pa. There does not seem to be a direct correlation, as mineral stability is a function of numerous factors, including kinetics (Hamad, 1976). Nevertheless our experimental results suggest that minerals such as gypsum and nontronite, both of which have been detected on Mars (Langevin et al., 2005; Poulet et al., 2005), have not undergone any excursions to pressures of a few Pa since their formation.

Future work in this area would ideally integrate several analytical techniques, such as reflectance spectroscopy, X-ray diffractometry, and evolved-gas analysis. Such approaches would allow better delineation of different alteration mechanisms such as dehydration and structural rearrangements, as well as quantifying the magnitude of volatile loss. Nevertheless, this study has shown that spectroscopic changes do accompany even short-duration exposures to martian surface conditions for a wide range of minerals.

Acknowledgments

This work was done at the University of Winnipeg's Planetary Spectrophotometer Facility (PSF) which was established with generous support from the Canada Foundation for Innovation, the Manitoba Research and Innovation Fund, and the Canadian Space Agency. We gratefully acknowledge the operational funding support provided by the Canadian Space Agency, the Natural Sciences and Engineering Research Council of Canada, and the University of Winnipeg. Thanks to Dr. Jeffrey Post of the Smithsonian Institution National Museum of Natural History for providing a number of the mineral samples used in this study. Thanks also to Mr. Neil Ball of the University of Manitoba Department of Geological Sciences for X-ray diffraction analysis of the samples. Dick Morris of NASA JSC kindly provided the palagonitic soil sample, and Mr. George Fulford of Alcan International provided the two hydroxide samples and associated analytical data. Thanks to Albert Yen for providing advice on calculating UV fluxes. Finally, special thanks to Janice Bishop and David Vaniman for their insightful and thorough reviews of this manuscript and many helpful comments.

References

Allen, C.C., Morris, R.V., 1999. Reply: Caution advised on suitability of a Mars soil stimulant. EOS Trans. AGU 80, 169.

Allen, C.C., Jager, K.M., Morris, R.V., Lindstrom, D.J., Lindstrom, M.M., Lockwood, J.P., 1998. Martian soil simulant available for scientific, educational study. EOS Trans. AGU 79, 405.

Bandfield, J.L., Glotch, T.D., Christensen, P.R., 2003. Spectroscopic identification of carbonate minerals in the martian dust. Science 301, 1084–1087.

Bell III, J.F., Wolff, M.J., James, P.B., Clancy, R.T., Lee, S.W., Martin, L.J., 1997. Mars surface mineralogy from Hubble Space Telescope imaging during 1994–1995: Observations, calibration, and initial results. J. Geophys. Res. 102, 9109–9123.

Bell III, J.F., Cloutis, E.A., Klassen, D.R., Clark, R.N., 2000. Spectroscopic evidence for diaspore (AlOOH) on Mars. Lunar Planet. Sci. 31. Abstract 1227 [CD-ROM].

Bibring, J.-P., Combes, M., Langevin, Y., Soufflot, A., Cara, C., Drossart, P., Encrenaz, Th., Erard, S., Forni, O., Gondet, B., Ksanfomality, L., Lellouch, E., Masson, Ph., Moroz, V.I., Rocard, F., Rozenqvist, J., Sotin, C., 1989. Results from the ISM experiment. Nature 341, 591–592.

Bibring, J.-P., Soufflot, A., Berthé, M., Langevin, Y., Gondet, B., Drossart, P., Bouyé, M., Combes, M., Puget, P., Semery, A., Bellucci, G., Formisano, V., Moroz, V., Kottsov, V., Bonello, G., Erard, S., Forni, O., Gendrin, A., Manaud, N., Poulet, F., Poulleau, G., Encrenaz, T., Fouchet, T., Melchiori, R., Altieri, F., Ignatiev, N., Titov, D., Zasova, L., Coradini, A., Capacionni, F., Cerroni, P., Fonti, S., Mangold, N., Pinet, P., Schmitt, B., Sotin, C., Hauber, E., Hoffmann, H., Jaumann, R., Keller, U., Arvidson, R., Mustard, J., Forget, F., 2004. OMEGA: Observatoire pour la Minéralogie, l'Eau, les Glaces et l'Activité. In: Wilson, A. (Ed.), Mars Express: The Scientific Payload. ESA SP-1240. ESA, Noordwijk, Netherlands, pp. 37–49.

Bichard, J.A., 1987. Oil Sands Composition and Behavior Research. AOSTRA Technical Publication Series, vol. 4. Alberta Oil Sands Technology and Research Authority, Edmonton, AB.

Bish, D.L., Scanlan, M.K., 2006. The hydration and dehydration of hydrous mixed-cation sulfates. Lunar Planet. Sci. 37. Abstract 1011 [CD-ROM].

Bish, D.L., Carey, J.W., Vaniman, D.T., Chipera, S.J., 2003. Stability of hydrous minerals on the martian surface. Icarus 164, 96–103.

Bishop, J.L., Pieters, C.M., 1995. Low-temperature and low atmospheric pressure infrared reflectance spectroscopy of Mars soil analog materials. J. Geophys. Res. 100, 5369–5379.

Bishop, J.L., Murad, E., Madejová, J., Komadel, P., Wagner, U., Scheinost, A.C., 1997. Visible, Mössbauer and infrared spectroscopy of dioctahedral smectites: Structural analyses of the Fe-bearing smectites Sampor, SWy-1 and SWa-1. In: Proc. 11th Int. Clay Conf., June 1997, pp. 413–419.

Bishop, J., Murad, E., Dyar, M.D., 2002. The influence of octahedral and tetrahedral cation substitution on the structure of smectites and serpentines as observed through infrared spectroscopy. Clay Miner. 37, 617–628.

Bishop, J.L., Murchie, S.L., Brown, A.J., Pelkey, S.M., Roach, L.A., Mustard, J.F., Bibring, J.P., CRISM Team, 2007. Sulfates in Juventae Chasma as seen by CRISM. Lunar Planet. Sci. 38. Abstract 2252 [CD-ROM].

Blaney, D.L., McCord, T.B., 1989. An observational search for carbonates on Mars. J. Geophys. Res. 94, 10159–10166.

Bonello, G., Berthet, P., d'Hendecourt, L., 2005. Identification of magnesium sulfate hydration state derived from NIR reflectance spectroscopy. Lunar Planet. Sci. 36. Abstract 1996 [CD-ROM].

Brophy, G.P., Scott, E.S., Snellgrove, R.A., 1962. Sulfate studies. II. Solid solution between alunite and jarosite. Am. Mineral. 47, 112–126.

Bruckenthal, E.A., 1987. The dehydration of phyllosilicates and palagonites: Reflectance spectroscopy and differential scanning calorimetry. M.Sc. thesis, University of Hawaii, Honolulu, HI.

Calvin, W.M., King, T.V.V., 1997. Spectral characteristics of iron-bearing phyllosilicates: Comparison to Orgueil (CI1), Murchison and Murray (CM2). Meteorit. Planet. Sci. 32, 693–701.

Calvin, W.M., King, T.V.V., Clark, R.N., 1994. Hydrous carbonates on Mars? Evidence from Mariner 6/7 infrared spectrometer and ground-based telescopic spectra. J. Geophys. Res. 99, 14659–14675.

Chipera, S.J., Vaniman, D.T., 2007. Experimental stability of magnesium sulfate hydrates that may be present on Mars. Geochim. Cosmochim. Acta 71, 241–250.

Chipera, S.J., Vaniman, D.T., Bish, D.L., Carey, J.W., Feldman, W.C., 2005. Experimental stability and transformation kinetics of magnesium sulfate hydrates that may be present on Mars. Lunar Planet. Sci. 36. Abstract 1497 [CD-ROM].

Chipera, S.J., Vaniman, D.T., Carey, J.W., 2006. Dehydration and metastable states of Mg-sulfate hydrates that may be present on Mars. Lunar Planet. Sci. 37. Abstract 1457 [CD-ROM].

Chipera, S.J., Vaniman, D.T., Bish, D.L., 2007. The effect of temperature and water on ferric-sulfates. Lunar Planet. Sci. 38. Abstract 1409 [CD- ROM].

Christensen, P.R., Morris, R.V., Lane, M.D., Bandfield, J.L., Malin, M.C., 2001. Global mapping of martian hematite mineral deposits: Remnants of water-driven processes on early Mars. J. Geophys. Res. 106, 23873–23885.

Clark, R.N., Roush, T.L., 1984. Reflectance spectroscopy: Quantitative analysis techniques for remote sensing applications. J. Geophys. Res. 89, 6329–6340.

Clark, R.N., King, T.V.V., Klejwa, M., Swayze, G., Vergo, N., 1990. High spectral resolution reflectance spectroscopy of minerals. J. Geophys. Res. 95, 12653–12680.

Cloutis, E.A., Bell III, J.F., 2000. Diaspores and related hydroxides: Spectral-compositional properties and implications for Mars. J. Geophys. Res. 105, 7053–7070.

Cloutis, E.A., Bell III, J.F., 2004. Mafic silicate mapping on Mars: Effects of palagonitic material, multiple mafic silicates, and spectral resolution. Icarus 172, 233–254.

Cloutis, E.A., Hawthorne, F.C., Mertzman, S.A., Krenn, K., Craig, M.A., Marcino, D., Methot, M., Strong, J., Mustard, J.F., Blaney, D.L., Bell III, J.F., Vilas, F., 2006. Detection and discrimination of sulfate minerals using reflectance spectroscopy. Icarus 184, 121–157.

Cockell, C.S., Catling, D.C., Davis, W.L., Snook, K., Kepner, R.L., Lee, P., McKay, C.P., 2000. The ultraviolet environment of Mars: Biological implications past, present, and future. Icarus 146, 343–359.

Craig, M., Cloutis, E.A., Mueller, T., 2001. ME and mini-ME: Two Mars environmental simulation chambers for reflectance spectroscopy. Lunar Planet. Sci. 32. Abstract 1368 [CD-ROM].

Crowley, J.K., 1991. Visible and near-infrared (0.4–2.5 μm) reflectance spectra of playa evaporate minerals. J. Geophys. Res. 96, 16231–16240.

Dalton III, J.B., 2003. Spectral behavior of hydrated sulfate salts: Implications for Europa mission spectrometer design. Astrobiology 3, 771–784.

Dollfus, A., Deschamps, M., Zimbelman, J.R., 1993. Soil texture and granulometry at the surface of Mars. J. Geophys. Res. 98, 3413–3429.

Eggleton, R.A., Tilley, D.B., 1998. Hisingerite: A ferric kaolin mineral with curved morphology. Clays Clay Miner. 46, 400–413.

Erard, S., Bibring, J.-P., Mustard, J., Forni, O., Head, J.W., Hurtrez, S., Langevin, Y., Pieters, C.M., Rosenqvist, J., Sotin, C., 1991. Spatial variations in composition of the Valles Marineris and Isidis Planitia regions of Mars derived from ISM data. Proc. Lunar Sci. Conf. 21, 437–455.

Erard, S., Lellouch, E., Encrenaz, Th., Morris, P., de Graauw, T., Burgdorf, M., 2000. Composition of martian surface materials and dust from ISO observations. Lunar Planet. Sci. 31. Abstract 1325 [CD-ROM].

Farmer, V.C., 1992. Possible confusion between so-called ferrihydrites and hisingerites. Clay Miner. 27, 373–378.

Freeman, J.J., Wang, A., Joliff, B.L., 2007a. $MgSO_4{\cdot}11H_2O$—Powder XRD, Raman and VIS-NIR spectroscopic characterization. Lunar Planet. Sci. 38. Abstract 1197 [CD-ROM].

Freeman, J.J., Wang, A., Joliff, B.L., 2007b. Pathways to form kieserite from epsomite at mid to low temperatures with relevance to Mars. Lunar Planet. Sci. 38. Abstract 1298 [CD-ROM].

Gendrin, A., Mangold, N., Bibring, J.-P., Langevin, Y., Gondet, B., Poulet, F., Bonello, G., Quantin, C., Mustard, J., Arvidson, R., LeMouélic, S., 2005. Sulfates in martian layered terrains: The OMEGA/Mars Express view. Science 307, 1587–1591.

Gooding, J.L., 1978. Chemical weathering on Mars: Thermodynamic stabilities of primary minerals (and their alteration products) from mafic igneous rocks. Icarus 33, 483–513.

Hamad, S.El.D., 1976. A study of the reaction $Na_2SO_4{\cdot}10H_2O \rightarrow Na_2SO_4 + 10H_2O$ in the temperature range 0 to 25 °C. Thermochim. Acta 17, 85–96.

Hamilton, V.E., McSween Jr., H.Y., Hapke, B., 2005. Mineralogy of martian atmospheric dust inferred from thermal infrared spectra of aerosols. J. Geophys. Res. 110, doi:10.1029/2005JE002501. E12006.

Hord, C.W., Barth, C.A., Pearce, J.B., 1970. Ultraviolet spectroscopy experiment for Mariner Mars 1971. Icarus 12, 63–77.

Howari, F.M., Goodell, P.C., Miyamoto, S., 2002. Spectral properties of salt crusts formed in saline soils. J. Environ. Qual. 31, 1453–1461.

Huguenin, R.L., 1974. The formation of goethite and hydrated clay minerals on Mars. J. Geophys. Res. 79, 3895–3905.

Hunt, J.M., 1979. Petroleum Geochemistry and Geology. Freeman, San Francisco, CA.

Hunt, G.R., Salisbury, J.W., Lenhoff, C.J., 1973. Visible and near infrared spectra of minerals and rocks. VI. Additional silicates. Mod. Geol. 4, 85–106.

Johnson, J.R., Bell III, J.F., Cloutis, E., Staid, M., Farrand, W.M., McCoy, T., Rice, M., Wang, A., Yen, A., 2007. Mineralogic constraints on sulfur-rich soils from Pancam spectra at Gusev crater, Mars. Geophys. Res. Lett. 34, doi:10.1029/2007GL029894. L13202.

Jouglet, D., Poulet, F., Milliken, R.E., Mustard, J.F., Bibring, J.-P., Langevin, Y., Gondet, B., Gomez, C., 2007. Hydration state of the martian surface as seen by Mars Express OMEGA. 1. Analysis of the 3 μm hydration feature. J. Geophys. Res. 112, doi:10.1029/2006JE002846. E08S06.

Karakassides, M.A., Gournis, D., Simopoulos, T., Petridis, D., 2000. Mössbauer and infrared study of heat-treated nontronite. Clays Clay Miner. 48, 68–74.

King, T.V.V., Clark, R.N., 1989. Spectral characteristics of chlorites and Mg-serpentines using high-resolution reflectance spectroscopy. J. Geophys. Res. 94, 13997–14008.

King, P.L., Lescinsky, D.T., Nesbitt, H.W., 2004. The composition and evolution of primordial solutions on Mars, with application to other planetary bodies. Geochim. Cosmochim. Acta 23, 4993–5008.

Klingelhöfer, G., Morris, R.V., Bernhardt, B., Schröder, C., Rodionov, D.S., de Souza Jr., P.A., Yen, A., Gellert, R., Evlanov, E.N., Zubkov, B., Foh, J., Bonnes, U., Kankeleit, E., Gütlich, P., Ming, D.W., Renz, F., Wdowiak, T., Squyres, S.W., Arvidson, R.E., 2004. Jarosite and hematite at Meridiani Planum from Opportunity's Mössbauer spectrometer. Science 306, 1740–1745.

Kuhn, W.R., Atreya, S.K., 1979. Solar radiation incident on the martian surface. J. Mol. Evol. 14, 57–64.

Lane, M.D., Bishop, J.L., Dyar, M.D., Parente, M., King, P.L., Hyde, B.C., 2007. Identifying the phosphate and ferric sulfate minerals in the Paso Robles soils (Gusev Crater, Mars) using an integrated spectral approach. Lunar Planet. Sci. 38. Abstract 2176 [CD-ROM].

Langevin, Y., Poulet, F., Bibring, J.P., Gondet, B., 2005. Sulfates in the north polar region of Mars detected by OMEGA/Mars Express. Science 307, 1584–1587.

Lellouch, E., Encrenaz, T., de Graauw, T., Erard, S., Morris, P., Crovisier, J., Feuchtgruber, H., Girard, T., Burgdorf, M., 2000. The 2.4–45 μm spectrum of Mars observed with the Infrared Space Observatory. Planet. Space Sci. 48, 1393–1405.

Madejová, J., Bujdák, J., Gates, W.P., Komadel, P., 1996. Preparation and infrared spectroscopic characterization of reduced-charge montmorillonite with various Li contents. Clay Miner. 31, 233–241.

Mang, G.-Q., 1988. Composition and structural characteristics of eastern and western oil shale. M.Sc. thesis, West Virginia Univ., Morgantown, WV, 91 pp.

Mao, H.K., Bell, P.M., 1974. Crystal-field effects of ferric iron in goethite and lepidocrocite. In: Band Assignment and Geochemical Applications at High Pressure, vol. 73. Carnegie Inst., Washington, DC, pp. 502–507.

Marion, G.M., Kargel, J.S., 2005. Stability of magnesium sulfate minerals in martian environments. Lunar Planet. Sci. 36. Abstract 2290 [CD-ROM].

Mertzman, S.A., 2000. K–Ar results from the southern Oregon–northern California cascade range. Oregon Geol. 62, 99–122.

Morris, R.V., Lauer Jr., H.V., Lawson, C.A., Gibson Jr., E.K., Nace, G.A., Stewart, C., 1985. Spectral and other physicochemical properties of submicron powders of hematite (α-FeOOH), maghemite (γ-Fe_2O_3), magnetite (Fe_3O_4), goethite (α-FeOOH), and lepidocrocite (γ-FeOOH). J. Geophys. Res. 90, 3126–3144.

Morris, R.V., Golden, D.C., Bell III, J.F., Shelfer, T.D., Scheinost, A.C., Hinman, N.W., Furniss, G., Mertzman, S.A., Bishop, J.L., Ming, D.W., Allen, C.C., Britt, D.T., 2000. Mineralogy, composition, and alteration of Mars Pathfinder rocks and soils: Evidence from multispectral, elemental, and magnetic data on terrestrial analogue, SNC meteorite, and Pathfinder samples. J. Geophys. Res. 105, 1757–1817.

Morris, R.V., Golden, D.C., Ming, D.W., Shelfer, T.D., Jørgensen, L.C., Bell III, J.F., Graff, T.G., Mertzman, S.A., 2001. Phyllosilicate-poor palagonitic dust from Mauna Kea Volcano (Hawaii): A mineralogical analogue for magnetic martian dust? J. Geophys. Res. 106, 5057–5083.

Mukhin, L.M., Koscheev, A.P., Dikov, Yu.P., Huth, J., Wänke, H., 1996. Experimental simulations of the photodecomposition of carbonates and sulfates on Mars. Nature 379, 141–143.

Murchie, S., Kirkland, L., Erard, S., Mustard, J., Robinson, M., 2000. Near-infrared spectral variations of martian surface materials from ISM imaging spectrometer data. Icarus 147, 444–471.

Murchie, S., Arvidson, R., Barnouin-Jha, O., Beisser, K., Bibring, J.-P., Bishop, J., Boldt, J., Choo, T., Clancy, R.T., Darlington, E.H., Des Marais, D., Fort, D., Hayes, J., Lees, J., Malaret, E., Mehoke, D., Morris, R., Mustard, J., Peacock, K., Robinson, M., Roush, T., Schaefer, E., Silverglate, P., Smith, M., Thompson, P., Tossman, B., 2002. CRISM: Compact Reconnaissance Imaging Spectrometer for Mars on the Mars Reconnaissance Orbiter. Lunar Planet. Sci. 33. Abstract 1697 [CD-ROM].

Mustard, J.F., Murchie, S., Erard, S., Sunshine, J., 1997. In situ compositions of martian volcanics: Implications for the mantle. J. Geophys. Res. 102, 25605–25615.

Mustard, J.F., Murchie, S.L., Pelkey, S.M., Ehlmann, B.L., Milliken, R.E., Grant, J.A., Bibring, J.-P., Poulet, F., Bishop, J.L., Roach, L.A., Seelos, F., Humm, D., CRISM Science Team, 2007. Overview of hydrated silicate minerals observed on Mars by CRISM. In: 7th Int. Mars Conf. Abstract 3240.

Navrotsky, A., Forray, F.L., Drouet, C., 2005. Jarosite stability on Mars. Icarus 176, 250–253.

O'Connor, J.T., 1968. Mineral stability at the martian surface. J. Geophys. Res. 73, 5301–5311.

Patel, M.R., Christou, A.A., Cockell, C.S., Ringrose, T.J., Zarnecki, J.C., 2004. The UV environment of the Beagle 2 landing site: Detailed investigations and detection of atmospheric state. Icarus 168, 93–115.

Pollack, J.B., Wilson, R.N., Goles, G.G., 1970. A re-examination of the stability of goethite on Mars. J. Geophys. Res. 75, 7491–7499.

Pollack, J.B., Roush, T., Witteborn, F., Bregman, J., Wooden, D., Stoker, C., Toon, O.B., Rank, D., Dalton, B., Freedman, R., 1990. Thermal emission spectra of Mars (5.4–10.5 μm): Evidence for sulfates, carbonates, and hydrates. J. Geophys. Res. 95, 14595–14627.

Post, J.L., Noble, P.N., 1993. The near-infrared combination band frequencies of dioctahedral smectites, micas, and illites. Clays Clay Miner. 41, 639–644.

Poulet, F., Bibring, J.P., Mustard, J.F., Gendrin, A., Mangold, N., Langevin, Y., Arvidson, R.E., Gondet, B., Gomez, C., Omega Team, 2005. Phyllosilicates on Mars and implications for early martian climate. Nature 438, 623–627.

Presley, M.A., Craddock, R.A., 2006. Thermal conductivity measurements of particulate materials. 3. Natural samples and mixtures of particle sizes. J. Geophys. Res. 111, doi:10.1029/2006JE0002706.

Prieto, A.C., Dubessy, J., Cathelineau, M., 1991. Structure–composition relationships in trioctahedral chlorites: A vibrational spectroscopy study. Clays Clay Miner. 39, 531–539.

Prieto-Ballesteros, O., Fernandez-Remolar, D., Mateo-Martí, E., Fernandez-Sampedro, M., Kargel, J.S., Friedlander, L.R., Martín-Gago, J.A., Arvidson, R.E., 2007. Phase stability experiments of hydrated magnesium sulfates at environmental conditions of martian surface. Lunar Planet. Sci. 38. Abstract 1512 [CD-ROM].

Robertson, K., Bish, D., 2007. The dehydration kinetics of gypsum: The effect of relative humidity on its stability and implications in the martian environment. Lunar Planet. Sci. 38. Abstract 1432 [CD-ROM].

Sherman, D.M., 1985. SCF-Xα-SW MO study of Fe–O and Fe–OH chemical bonds: Applications to the Mössbauer spectra and magnetochemistry of hydroxyl-bearing Fe^{3+} oxides and silicates. Phys. Chem. Miner. 12, 311–314.

Sherman, D.M., Vergo, N., 1988. Optical (diffuse reflectance) and Mössbauer spectroscopic study of nontronite and related Fe-bearing smectites. Am. Mineral. 73, 1346–1354.

Sherman, D.M., Burns, R.G., Burns, V.M., 1982. Spectral characteristics of the iron oxides with application to the martian bright region mineralogy. J. Geophys. Res. 87, 10169–10180.

Shirozu, H., 1980. Cation distribution, sheet thickness, and O–OH space in trioctahedral chlorites and X-ray and infrared study. Mineral. J. 10, 14–34.

Sinton, W.M., 1959. Further evidence of vegetation on Mars. Science 130, 1234–1237.

Stoffregen, R.E., Alpers, C.N., Jambor, J.L., 2000. Alunite–jarosite crystallography, thermodynamics and geochronology. In: Alpers, C.N., Jambor, J.L., Nordstrom, D.K. (Eds.), Sulfate Minerals. In: Reviews in Mineralogy and Geochemistry, vol. 40. Min. Soc. Am., Washington, DC, pp. 453–479.

Vaniman, D.T., Chipera, S.J., 2006. Transformations of Mg- and Ca-sulfate hydrates in Mars regolith. Am. Mineral. 91, 1628–1642.

Vaniman, D.T., Bish, D.L., Chipera, S.J., Fialips, C.I., Carey, J.W., Feldman, W.C., 2004. Magnesium sulfate salts and the history of water on Mars. Nature 431, 663–665.

Vaniman, D.T., Chipera, S.J., Bish, D.L., Carey, J.W., Feldman, W.C., 2005. Martian relevance of dehydration and rehydration in the Mg-sulfate system. Lunar Planet. Sci. 36. Abstract 1486 [CD-ROM].

Vaniman, D.T., Chipera, S.J., Carey, J.W., 2006. Hydration experiments and physical observations at 193 K and 243 K for Mg-sulfates relevant to Mars. Lunar Planet. Sci. 37. Abstract 1442 [CD-ROM].

Wang, A., Freeman, J.J., Joliff, B.L., Chou, I.-M., 2006a. Sulfates on Mars, a systematic Raman spectroscopic study of hydration states of magnesium sulfates. Lunar Planet. Sci. 37. Abstract 2191 [CD-ROM].

Wang, A., Freeman, J.J., Joliff, B.L., Arvidson, R.E., 2006b. Conversion of crystalline $MgSO_4 \cdot xH_2O$ to the hydrated amorphous phase—A Raman, NIR, and XRD study. Lunar Planet. Sci. 37. Abstract 2168 [CD-ROM].

Wang, A., Freeman, J.J., Joliff, B.L., 2007. Formation rate of amorphous magnesium sulfates at low temperatures approaching the current surface conditions on Mars. Lunar Planet. Sci. 38. Abstract 1195 [CD-ROM].

White, W.B., Keester, K.L., 1966. Optical absorption spectra of iron in the rock-forming silicates. Am. Mineral. 51, 774–791.

Xu, W., Tosca, N.J., McLellan, S.M., Parise, J.B., 2007. Relative humidity-induced phase transitions of Fe-sulfate minerals: In situ X-ray diffraction studies. Lunar Planet. Sci. 38. Abstract 1860 [CD-ROM].

Yen, A.S., Murray, B., Rossman, G.R., Grunthaner, F.J., 1999. Stability of hydroxylated minerals on Mars: A study on the effects of exposure to ultraviolet radiation. J. Geophys. Res. 104, 27031–27041.

Yen, A.S., Kim, S.S., Hecht, M.H., Frant, M.S., Murray, B., 2000. Evidence that the reactivity of the martian soil is due to superoxide ions. Science 289, 1909–1912.